Forces and Torque acting on a Rudder while Manoeuvring

Guillaume Delefortrie*[1,2], Wim Van Hoydonck[1], Katrien Eloot[1]

[1]Flanders Hydraulics Research, Berchemlei 115, 2140 Antwerp, Belgium

[2]Ghent University, Maritime Technology Division, Technologiepark 60, 9052 Ghent, Belgium

*Corresponding author: Guillaume.Delefortrie@mow.vlaanderen.be

Abstract

The present paper introduces a mathematical model applicable to force and torque prediction on a rudder in behind hull/propeller conditions for a ship performing manoeuvres in a harbour. The latter implies a full 360° possible inflow direction to the rudder, combined with propeller rates ahead or astern. The mathematical model coefficients were derived based on a captive model test campaign performed with the benchmark container hull KCS and is being successfully applied in the ship manoeuvring simulators at Flanders Hydraulics Research. The results will internationally help model based research on ship manoeuvring in shallow and confined water.

Keywords

Rudder, inflow, propeller, lift, drag, torque

List of Symbols

A_B	balancing rudder area	m²
A_R	total rudder area	m²
b	rudder height	m
B	breadth	m
$\bar{c}$	average rudder chord	m
c_P	centre of pressure	m
$c_{P\bar{c}}$	distance rudder leading edge to c_P	m
C_D	drag coefficient	-
C_L	lift coefficient	-
C_Q	torque coefficient	-
C_T	thrust coefficient	-
d	distance rudder leading edge to stock	m
D	drag	N
D_P	propeller diameter	m
F_N	force, perpendicular to the rudder	N
F_Q	torque about rudder stock	Nm
F_T	tangential rudder force	N
F_X	longitudinal rudder force	N

F_Y	lateral rudder force	N
$\overline{GM}$	initial transverse stability lever	m
g	gravity acceleration	m/s²
h	water depth	m
$\bar{\boldsymbol{I}}$	inertia tensor	kgm²
I_{**}	moment or product of inertia	kgm²
J	propeller advance rate	-
k_{Hr}	flow straightening factor (yaw)	-
k_{Hv}	flow straightening factor (drift)	-
K_m	propeller jet contraction	-
K_T	propeller thrust coefficient	-
L	lift	N
$L_{(PP)}$	length (between perpendiculars)	m
M	steering engine torque	Nm
m	ship's mass	kg
N	yaw moment	Nm
n	propeller rate	1/s
Q_{SG}	torque delivered by steering gear	Nm
R	position rudder stock; propeller radius	m
r	yaw velocity	rad/s
	radius	m
T	draft	m
	period	s
t	time	s
$\bar{t}$	average rudder thickness	m
T_P	propeller thrust	N
u	longitudinal ship velocity	m/s
u_P	longitudinal velocity near propeller	m/s
u_R	longitudinal velocity near rudder	m/s
u_{R0}	hull component of the longitudinal velocity near rudder	m/s
u_{RP}	propeller component of the longitudinal velocity near rudder	m/s
ukc	under keel clearance	
V	total ship velocity	m/s
V_R	total ship velocity near rudder	m/s
v	lateral ship velocity	m/s
v_R	lateral velocity near rudder	m/s
w_R	wake factor for the rudder	-
w_T	wake factor for the thrust	-
X	longitudinal force	N
x	longitudinal coordinate	m
x_G	longitudinal centre of gravity	m
Y	sway force	N
y	lateral coordinate	m
y_G	lateral centre of gravity	m
z_G	vertical centre of gravity	m
α	inflow angle	deg
β	drift angle	deg
β_R	drift angle near rudder	deg
γ	yaw angle	deg

γ^*	propeller loading angle for yaw	deg
δ	rudder angle	deg
δ_0	rudder asymmetry correction	deg
$\varepsilon^{(*)}$	(apparent) propeller loading angle	deg
ζ	ratio of rudder wake and propeller wake	-
η	propeller diameter ÷ rudder height	-
ξ	parameter	-
ρ	water density	kg/m³
φ_*	phase angle	deg
χ	yaw-drift correlation angle	deg
ψ	course angle	deg

Subscripts

a	amplitude
m	mean
meas	measured
mod	modelled
P	propeller
PS	portside
R	rudder
SS	starboard side

Superscripts

.	time derivative

1 Introduction

The Knowledge Centre for Manoeuvring in Shallow and Confined Water (co-operation Flanders Hydraulics Research & Ghent University) is particularly concerned with the manoeuvring behaviour of ships in difficult environments. The assessment of this manoeuvring behaviour is typically conducted in virtual conditions provided by the digital environment of a ship manoeuvring simulator. The realism of the simulations depend however heavily on the quality of the prediction of the manoeuvring forces.

The base definition of manoeuvrability is the ease with which a ship can change its course. This course change can be performed with external aids, such as tug boats, but most of the time the ship will need to rely on its own devices, which in its most basic form is a rudder and/or thruster. A rudder is a hydrofoil shape that when located in an oblique inflow generates a lift and drag force. The lift is the useful component and provides a lateral force at the stern of the ship generating a yawing moment, which in turn changes the course of the ship. The lift being generated depends on a number of parameters; the most important ones are the hydrofoil shape, the angle of attack of the flow and the inflow velocity. A good base work in this respect that can be recommended is the book of Molland and Turnock (2007).

The effect of the hydrofoil shape will not be discussed further in this article. Some recent examples of shape studies can be found in Yang et al. (2015) and Hasanvand et al. (2019). Instead the focus will be put on the effect of the angle of attack of the flow and its magnitude. The latter is already quite

complex to predict, because the rudder is located within the wake field of the ship and within the jet of the propeller. Both wake field and propeller jet are influenced by the manoeuvring of the ship in terms of sailing speeds and propeller revolutions. A practical way to deal with this is to estimate the velocity of the propeller jet by means of the momentum theory of the propeller. This is typically applied in the manoeuvring models of the MMG group, see for instance Yasukawa and Yoshimura (2015), however limited to flow predictions when the ship is sailing ahead and the propeller turns ahead and thus assists the motion of the ship; a condition which is commonly referred to as the first quadrant when the signs of propeller rate n and ship's longitudinal speed u are considered:

- Quadrant 1: $u \geq 0; n \geq 0$
- Quadrant 2: $u \geq 0; n < 0$
- Quadrant 3: $u < 0; n \leq 0$
- Quadrant 4: $u < 0; n > 0$

Shen and Hughes (2012) extend the flow prediction considering the effects of propeller jet contraction and tangential flow generated by the propeller, however, also they limited themselves to the first quadrant. Their bibliography is nevertheless interesting for readers who want to have more information on rudder inflow.

It is clear that literature on the inflow of the rudder is rather scarce and even more when 4 quadrants are considered. To the authors' best knowledge only two papers were published on this topic during the last decade. The first one is by Hwang (2012), who elaborates on the inflow predictions in the different quadrants and especially depicts the problems with flow coming from opposite directions in the even quadrants. According to him, CFD research should be a useful means to solve this problem. A second publication by Häusler et al. (2015) does not even consider the rudder, but discusses the propeller jet in four quadrants operation, however, providing some useful insights which are based on helicopter theory.

A vaster amount of numerical research was published in the last decade on this topic. This numerical research either focused on the prediction of lift and drag in open water conditions (without hull or propeller), such as Van Hoydonck et al. (2018), or looks at the effects of hull and propeller on the inflow to the rudder. Methods can vary from simple to complex, and are mostly referred to as hybrid methods because they consider a combination of potential flow methods with a viscous CFD solver. Examples of such approach are given by Calcagni et al. (2017); Mofidi et al. (2018) or Su et al. (2018). Due to the computational expenses, numerical methods mostly investigate a singular problem, such as the rudder performance in bollard pull conditions (Villa et al., 2018) or interaction problems in inland navigation (Kaidi et al., 2018) and can thus not readily be applied in ship manoeuvring simulations.

The present paper intends to discuss the inflow to the rudder behind the propeller and behind the hull in full four quadrants conditions and for a full drift and yaw range, which are conditions that a ship may encounter in a harbour environment and thus in shallow water areas. A method is presented to predict the lift and drag of the rudder in such conditions and the steering torque as well. This method is tested against experiments that have been carried out in the Towing Tank for Manoeuvres in Confined Water over the past years and was applied to different ship models. In the present paper the method is exemplified with the well-known benchmark hull KCS. The effect of the rudder induced forces on the ship itself falls out of the scope of this paper and is left for future work, but interested readers can consult Yasukawa and Yoshimura (2015) or Fukui (2012) to have an idea of the present state of the art.

2 Mathematical formulation

To set the ideas, first a mathematical description of the forces and torque acting on the rudder is given. Figure 1 shows the used ship-fixed coordinate system $Oxyz$ with origin amidships on the calm water plane and horizontally bound to that plane. In the present paper, the rudder angle is considered positive for excursions to portside, and a right handed propeller is used. Figure 2 shows the forces acting on a rudder in uniform inflow and Figure 3 shows an example of the propagation of these forces to the ship fixed axis system in ship manoeuvring motion.

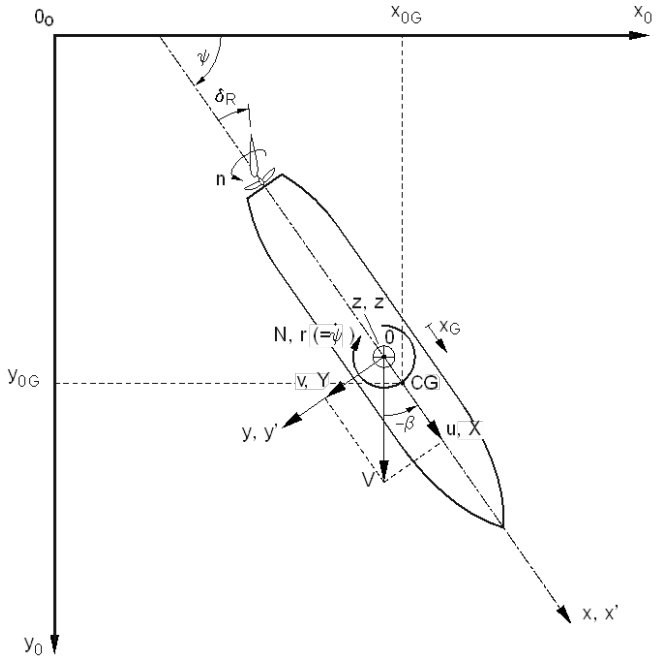

Figure 1 – Sign conventions and coordinate systems.

Important hydrodynamic angles which relate the surge velocity u, the sway velocity v and the yaw rate r of the ship are the drift angle:

$$\beta = \arctan\left(\frac{-v}{u}\right) \tag{2.1}$$

and the yaw angle:

$$\gamma = \arctan\left(\frac{0.5rL}{u}\right) \tag{2.2}$$

The range of the $\arctan$ function in this research is extended to [-π,π] for four quadrants.

The forces acting on the rudder behind the hull or propeller are based on the open water characteristics of the rudder. To determine the open water lift and drag coefficients of the rudder, tests have been carried out with solely the rudder for a variety of inflow angles α (Figure 4). More information on this procedure can be found in Van Hoydonck et al. (2018). When the rudder is behind the ship the inflow is affected, which is modelled with the effective rudder angle and drift near the rudder:

$$\alpha = \delta + \delta_0 + \beta_R \tag{2.3}$$

δ_0 (the rudder angle where the normal force F_N acting on the rudder becomes zero) is an offset for flow asymmetry:

$$\delta_0 = -\delta(F_N = 0) \tag{2.4}$$

β_R is the local drift angle at the rudder:

$$\beta_R = \arctan\left(\frac{-v_R}{u_R}\right) \tag{2.5}$$

u_R, v_R being the longitudinal and transverse component of the total horizontal flow velocity near the rudder:

$$V_R = \sqrt{u_R^2 + v_R^2} \tag{2.6}$$

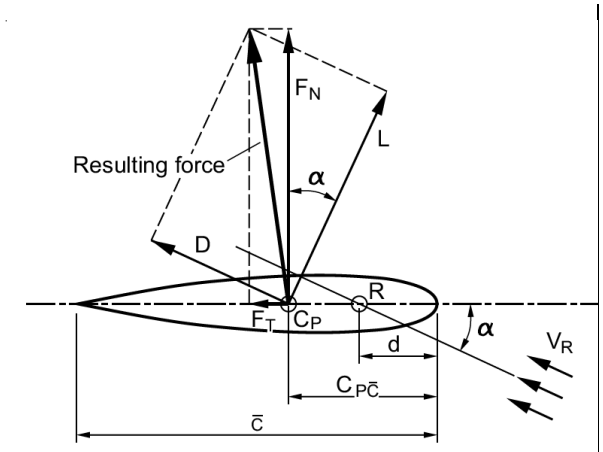

Figure 2 – Forces acting on a rudder in uniform inflow.

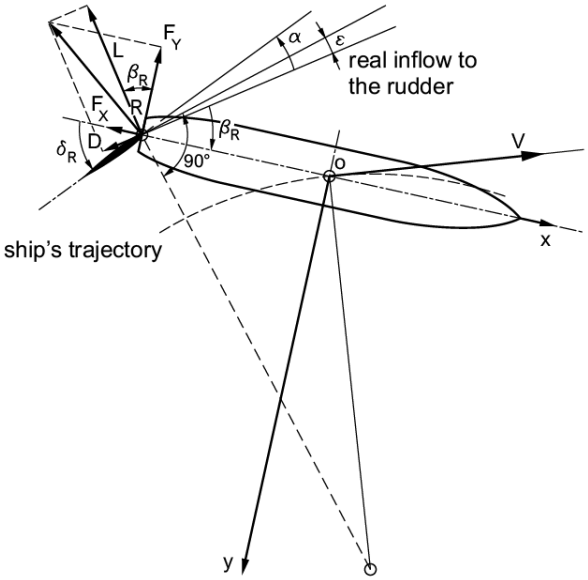

Figure 3 – Forces acting on a rudder behind a manoeuvring ship. In this example F_X and F_Y have negative force magnitudes when expressed in the ship fixed axis system. ε represents here the effective inflow angle to the rudder affected by manoeuvring motion and propeller rate.

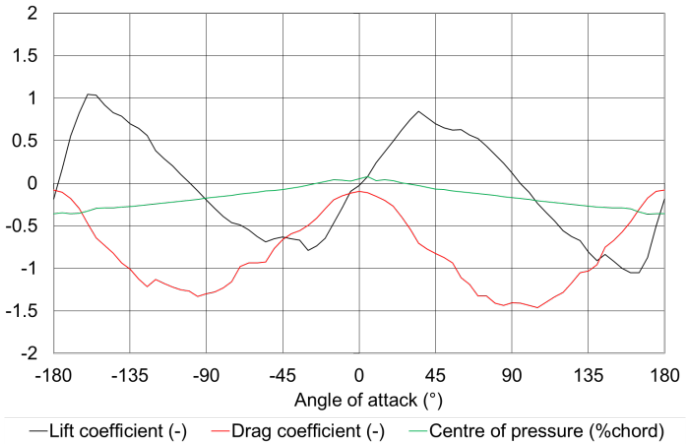

Figure 4 – Experimentally determined open water characteristic of the KCS rudder. The centre of pressure is expressed as a fraction of the chord length, 0 corresponding to the middle chord position.

Hence, the forces on the rudder can be expressed as:

$$F_X = \frac{1}{2}\rho A_R V_R^2 [C_L \sin\beta_R + C_D \cos\beta_R] \quad (2.7)$$

$$F_Y = \frac{1}{2}\rho A_R V_R^2 [C_L \cos\beta_R - C_D \sin\beta_R] \quad (2.8)$$

with F_X and F_Y oriented along the ship's longitudinal and lateral axis respectively.

The application point of the lateral force F_Y, or the centre of pressure, causes a moment about the rudder stock:

$$F_Q = c_P F_Y = \frac{1}{2}\rho c_P A_R V_R^2 [C_L \cos\beta_R - C_D \sin\beta_R] \quad (2.9)$$

which needs to be counteracted by the steering gear.

The modelling of the rudder forces is then reduced to the correct predictions of the inflow velocities to the rudder and the modelling of the torque to the correct prediction of the centre of pressure. Mind that the word 'reduction' does certainly not imply a simplification. To set the ideas the theoretical inflow velocity to the rudder will be determined in a next section, but first the experimental data used to derive the coefficients are introduced.

3 Experimental campaign

The coefficients of the mathematical model for the rudder forces and torque are in the present paper determined by an extensive experimental campaign of captive model tests with the benchmark container ship KCS. This ship is one of the ships considered at the SIMMAN workshops and the authors have submitted results (Delefortrie et al., 2020) to the delayed workshop SIMMAN 2021 based on the rudder force predictions considered in this article. The ship's particulars at model scale are shown in Table 1. The tests have been executed in the Towing Tank for Manoeuvres in Confined Water (Flanders Hydraulics Research, in co-operation with Ghent University, see Delefortrie et al. (2016) for more information on this tank) in 2017 at four different under keel clearances, corresponding to 100%, 50%, 20% and 10% of the ship's draft.

During the tests the ship was always equipped with rudder and propeller. The rudder of the KCS consists of a movable blade and a fixed horn. A rudder angle applies only to the blade. The common open water program executed for any ship with a single propeller and single rudder was extended with forced roll tests and tests at discrete heel angles different from zero, yielding more than 400 captive model tests per water depth, which cover the whole range of possible harbour manoeuvres (full range of drift and yaw angles, combined with ahead and astern propulsion).

Table 1 – Ship's main particulars (scale factor 1/52.667)

Parameter	Model scale	Full scale	Parameter	Model scale	Full scale
L_{PP} [m]	4.367	230.0	A_R [m²] Full Movable part	0.0196 0.0147	54.45 40.78
B [m]	0.611	32.2	Profile type	NACA 0018	
T [m]	0.2051	10.8	A_B [m²]	0.0049	13.62
$\overline{GM}$ [m]	0.049 (±0.003)	2.56	b [m]	0.1880	9.90
x_G [m]	-0.071 (±0.002)	-3.74	$\bar{c}$ [m]	0.1044	5.50
I_{XX} [kgm²]	15.2 (±1)	6.16E+09	$\bar{t}$ [m]	0.0188	0.99
I_{YY} [kgm²]	390.1 (±2)	1.58E+11	Aspect ratio	1.80	1.80
I_{ZZ} [kgm²]	409.6 (±2)	1.66E+11	Rudder stock diameter [m]	0.0171	0.9
D_P [m]	0.150	7.9			

4 Prediction of the inflow to the rudder

4.1 Theoretical derivation for the longitudinal inflow based on momentum theory

As in the MMG model, the momentum theory is used to derive the expressions for the longitudinal inflow to the rudder, however, here in four quadrants. The actual derivation of the expressions is given in Appendix 1. Here it suffices to say that instead of the more common use of the thrust coefficient K_T and advance rate J in the expressions, C_T and ε are used to avoid infinite values while crossing quadrants. C_T is a dimensionless thrust coefficient so that the propeller thrust is equal to:

$$T_P = \frac{0.7^2}{8}\pi^3\rho n^2 D_P^4 C_T(\varepsilon)(1+\tan^2\varepsilon) \tag{4.1}$$

with the propeller loading angle is:

$$\varepsilon = \arctan\left(\frac{(1-w_T)u}{0.7\pi n D_P}\right) \tag{4.2}$$

expressed in a [-180°,180°] range. The apparent propeller loading angle is:

$$\varepsilon^* = \arctan\left(\frac{u}{0.7\pi n D_P}\right) \tag{4.3}$$

The wake factor $w_T < 1$ can be determined based on application of the thrust identity on model test results. The different quadrants can be expressed as a function of ε or ε^* as well:

- Quadrant 1: ε, $\varepsilon^* \epsilon\ [0°, 90°]$;
- Quadrant 2: ε, $\varepsilon^* \epsilon\ (90°, 180°)$;
- Quadrant 3: ε, $\varepsilon^* \epsilon\ [-180°, -90°]$;
- Quadrant 4: ε, $\varepsilon^* \epsilon\ (-90°, 0°)$.

The expression for the inflow velocity in the first quadrant is then:

$$u_R = \zeta \sqrt{\left[\eta\left[\left(1-\frac{K_m}{\zeta}\right)\sin\varepsilon + \frac{K_m}{\zeta}\left(\sqrt{\sin^2\varepsilon + C_T}\right)\right]^2 + (1-\eta)\sin^2\varepsilon\right] \cdot [(0.7\pi n D_P)^2 + [(1-w_T)u]^2]} \tag{4.4}$$

In the second quadrant, the problem occurs of opposite flows generated by ship's motion and propeller. The dominant flow direction can be found by the following condition (see Appendix 1):

$$\left|(\zeta + 1 - K_m)\sin\varepsilon - (1-K_m)\sqrt{\sin^2\varepsilon + |C_T|}\right| \geq \zeta\sqrt{\frac{1-\eta}{\eta}}|\sin\varepsilon| \tag{4.5}$$

If the condition is met, the inflow velocity is given by:

$$u_R = \zeta \mathrm{sign}(u_{RP}) \sqrt{\left[\eta\left[\left(1+\frac{1-K_m}{\zeta}\right)\sin\varepsilon - \frac{1-K_m}{\zeta}\left(\sqrt{\sin^2\varepsilon + |C_T|}\right)\right]^2 + \mathrm{sign}(u_{RP})(1-\eta)\sin^2\varepsilon\right] \cdot [(0.7\pi n D_P)^2 + [(1-w_T)u]^2]} \tag{4.6}$$

In the other case the expression is

$$u_R = \zeta \sqrt{\left[\mathrm{sign}(u_{RP})\eta\left[\left(1+\frac{1-K_m}{\zeta}\right)\sin\varepsilon - \frac{1-K_m}{\zeta}\left(\sqrt{\sin^2\varepsilon + |C_T|}\right)\right]^2 + (1-\eta)\sin^2\varepsilon\right] \cdot [(0.7\pi n D_P)^2 + [(1-w_T)u]^2]} \tag{4.7}$$

The sign of u_{RP} is evaluated with:

$$u_{RP} = \left[(\zeta + 1 - K_m)\sin\varepsilon - (1-K_m)\sqrt{\sin^2\varepsilon + |C_T|}\right]\sqrt{[(0.7\pi n D_P)^2 + [(1-w_T)u]^2]} \tag{4.8}$$

Application of momentum theory in the third quadrant yields the expression:

$$u_R = -\zeta \sqrt{\left[\eta\left[-\sin\varepsilon + \frac{(1-K_m)}{\zeta}\left(\sqrt{\sin^2\varepsilon + |C_T|} + \sin\varepsilon\right)\right]^2 + (1-\eta)\sin^2\varepsilon\right] \cdot [(0.7\pi n D_P)^2 + [(1-w_T)u]^2]} \tag{4.9}$$

In the fourth quadrant again the dominant direction must be determined. If the following condition is met:

$$\left|(\zeta + K_m)\sin\varepsilon + K_m\sqrt{\sin^2\varepsilon + |C_T|}\right| \geq \zeta\sqrt{\frac{1-\eta}{\eta}}|\sin\varepsilon| \tag{4.10}$$

the inflow velocity is given by

$$u_R = \zeta \text{sign}(u_{RP}) \sqrt{\left[\eta\left[\left(1+\frac{K_m}{\zeta}\right)\sin\varepsilon + \frac{K_m}{\zeta}\left(\sqrt{\sin^2\varepsilon + |C_T|}\right)\right]^2 - \text{sign}(u_{RP})(1-\eta)\sin^2\varepsilon\right] \cdot [(0.7\pi n D_P)^2 + [(1-w_T)u]^2]} \quad (4.11)$$

In the other case the expression is

$$u_R = -\zeta \sqrt{\left|\text{sign}(u_{RP})\eta\left[\left(1+\frac{K_m}{\zeta}\right)\sin\varepsilon + \frac{K_m}{\zeta}\left(\sqrt{\sin^2\varepsilon + |C_T|}\right)\right]^2 - (1-\eta)\sin^2\varepsilon\right| \cdot [(0.7\pi n D_P)^2 + [(1-w_T)u]^2]} \quad (4.12)$$

The sign of u_{RP} is evaluated with:

$$u_{RP} = \left[(\zeta + K_m)\sin\varepsilon + K_m\sqrt{\sin^2\varepsilon + |C_T|}\right]\sqrt{[(0.7\pi n D_P)^2 + [(1-w_T)u]^2]} \quad (4.13)$$

For a continuous model, it is necessary to check the limiting conditions. Without propeller action the inflow speed to the rudder is given by

$$u_R = (1-w_R)u \quad (4.14)$$

In bollard pull conditions this inflow speed is:

- For positive propeller rates
$$u_R = 0.7\pi n D_P K_m \sqrt{\eta C_T} \quad (4.15)$$
- For negative propeller rates
$$u_R = 0.7\pi n D_P (1-K_m)\sqrt{\eta |C_T|} \quad (4.16)$$

4.2 Investigation of the bollard pull condition

In the first place the lateral rudder force is investigated in bollard pull condition, which allows the use of the simplified formulae (4.15) or (4.16) for the inflow speed. The lateral rudder force is then, for instance for positive propeller rate:

$$F_Y = \frac{1}{2}\rho A_R \eta C_T C_L (0.7\pi n D_P)^2 K_m^2 \quad (4.17)$$

The only unknown parameter in this equation is K_m. Figure 5 shows the *measured* K_m values as a function of the rudder angle, for different propeller rates for the KCS. The values around 5° are spreading around, because of the zero crossing of the lateral force, but in general a significantly smaller value of K_m is observed, which seems to depend on the rudder angle. It is plausible that the jet contraction depends on the position of the rudder with regards to the propeller, but not only the longitudinal position plays a role, but also its orientation with respect to the propeller. K_m should definitely be modelled as a function of the rudder angle, however, a separate function seems necessary for the longitudinal and lateral force.

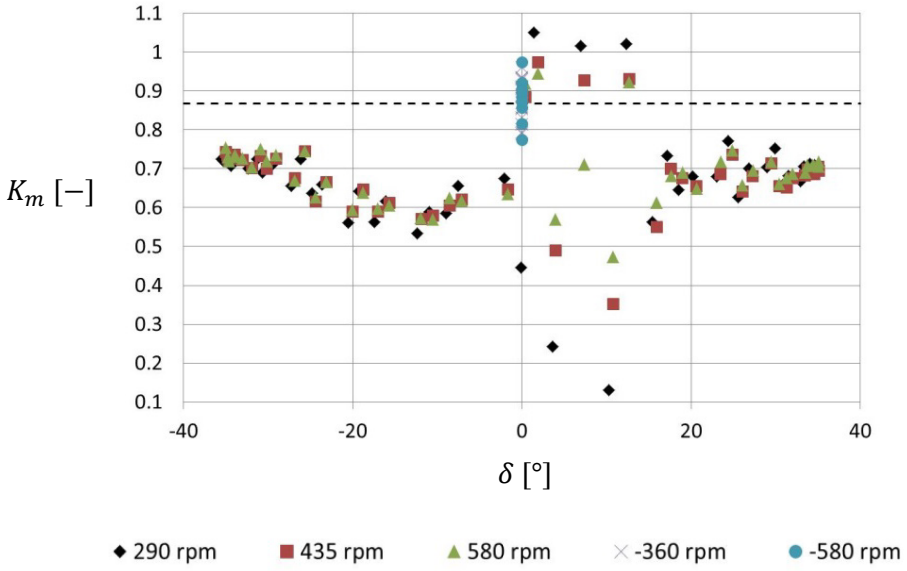

Figure 5 – Analytically computed values for K_m, based on the measured lateral rudder force, 50% ukc, bollard pull, KCS

4.3 Longitudinal inflow in the first quadrant

Given the fact that K_m should be a function of the rudder angle, the inflow speed in the first quadrant becomes:

$$u_R = \zeta(\varepsilon^*, \delta)\sqrt{\left[\eta\left[\left(1-\frac{K_m(\delta)}{\zeta(\varepsilon^*,\delta)}\right)\sin\varepsilon + \frac{K_m(\delta)}{\zeta(\varepsilon^*,\delta)}\left(\sqrt{\sin^2\varepsilon + C_T(\varepsilon)}\right)\right]^2 + (1-\eta)\sin^2\varepsilon\right] \cdot \left[(0.7\pi n D_P)^2 + \left[\left(1-w_T(\varepsilon^*)\right)u\right]^2\right]} \quad (4.18)$$

This inflow speed has been used to model $K_m(\delta)$ and $\zeta(\varepsilon^*)$ in the first quadrant. When considering only the first quadrant it may be debated which parameters affect the wake factor for the rudder. It seems however plausible that it follows the same trend as for the wake factor for the propeller:

$$\zeta(\varepsilon^*) = \frac{1-w_R(\varepsilon^*)}{1-w_T(\varepsilon^*)} \quad (4.19)$$

The wake factors for the rudder are depicted in Figure 6 b and c. Because the wake factor fully acts on the parameter ζ, the wake factor for the thrust has been added as well in Figure 6 a. The reader is pointed towards the apparent resemblance for the wake factors, which has a physical background. Nevertheless, the wake factor for the (longitudinal) rudder (force) shows some ostensible extremes at near bollard pull conditions.

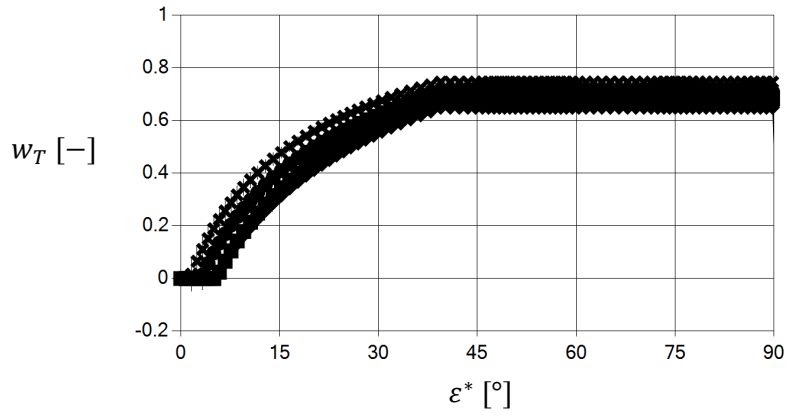

a. Thrust

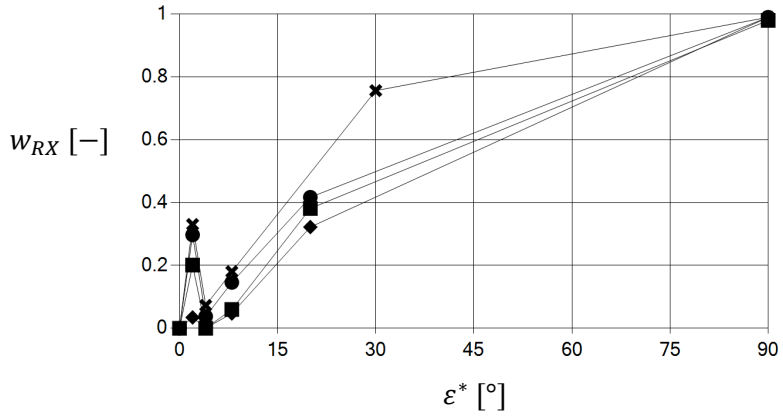

b. Longitudinal rudder force

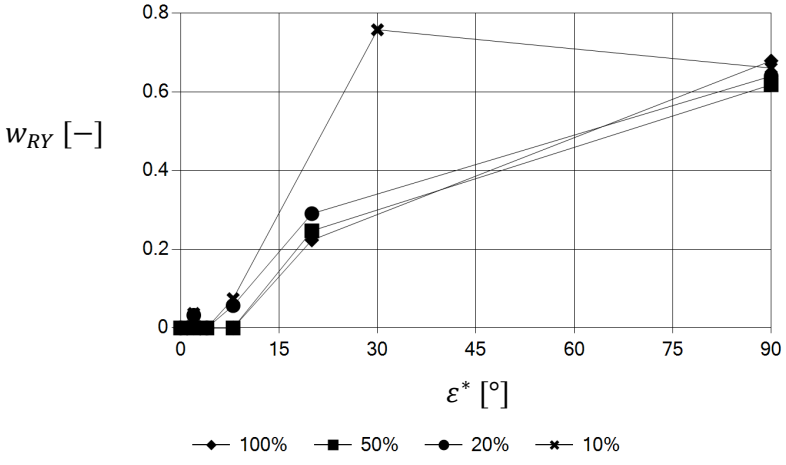

c. Lateral rudder force

Figure 6 – Wake factors, all ukc, KCS

To have a better understanding of the effect of w_R or ζ on the inflow speed, the factor

$$\zeta\sqrt{\left[\eta\left[\left(1-\frac{K_m}{\zeta}\right)\sin\varepsilon+\frac{K_m}{\zeta}\left(\sqrt{\sin^2\varepsilon+C_T}\right)\right]^2+(1-\eta)\sin^2\varepsilon\right]} \qquad (4.20)$$

contained in equation (4.4) has been plotted for two different ε^* values in Figure 7. With increasing ε^* value the sensitivity of ζ on the inflow speed will clearly increase. This is also confirmed by the fact that at bollard pull conditions, eq. (4.15), ζ has no effect on the inflow speed. In other words, larger variations of w_R are needed in near bollard pull conditions to have a significant effect of the inflow speed, which turns the ostensible extremes of w_R into mathematical artefacts rather than into a physical flow.

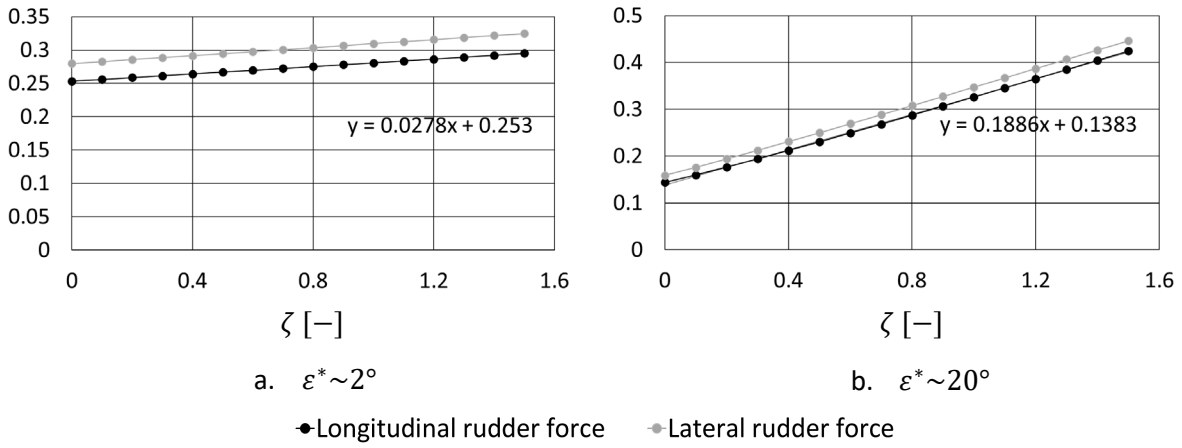

Figure 7 – Sensitivity of ζ on the inflow to the rudder, KCS, 100% ukc: the dimensionless result of equation (4.20) is plotted as a function of ζ

In the above expressions for the inflow velocity many parameters are considered to be solved by regression analysis, such as:

- K_m: a parameter which determines the change in size of the cross section of the propeller jet near the rudder. Because the jet is mostly contracted, $K_m < 1$ and is referred to as the contraction coefficient. This contraction coefficient seems to depend on the rudder angle, which could be caused by the specific orientation of the rudder with respect to the propeller jet;
- w_R: the wake factor near the rudder. In a simple approximation this wake factor could be taken equal to the wake factor near the propeller, however, it seems mostly different, but is also expressed as a function of the apparent propeller loading angle ε^*;
- η: initially a static parameter describing the ratio of the propeller diameter over the rudder height. However in practice a significant vertical variation of the flow in the propeller jet occurs, see for instance Figure 8 (here shown with yet another benchmark hull covered in SIMMAN 2021: the KVLCC2 tanker). This parameter η is important as it determinates the average inflow to the rudder:

  $$u_R = \sqrt{\eta u_{RP}^2 + (1-\eta)u_{R0}^2} \qquad (4.21)$$

  It is therefore better to consider η as a regression coefficient, yielding remarkably better results. In general lower values of η are needed for the longitudinal rudder force compared to the lateral rudder force.
- δ_0: the rudder angle where the normal force F_N acting on the rudder becomes zero. The water depth has a minor influence on the neutral rudder angles for the single rudder ships, but a

significant one for twin rudder ships. As for the multiplication of η, it was decided to maintain the different neutral rudder angles for each rudder and each force direction in the mathematical model formulation.

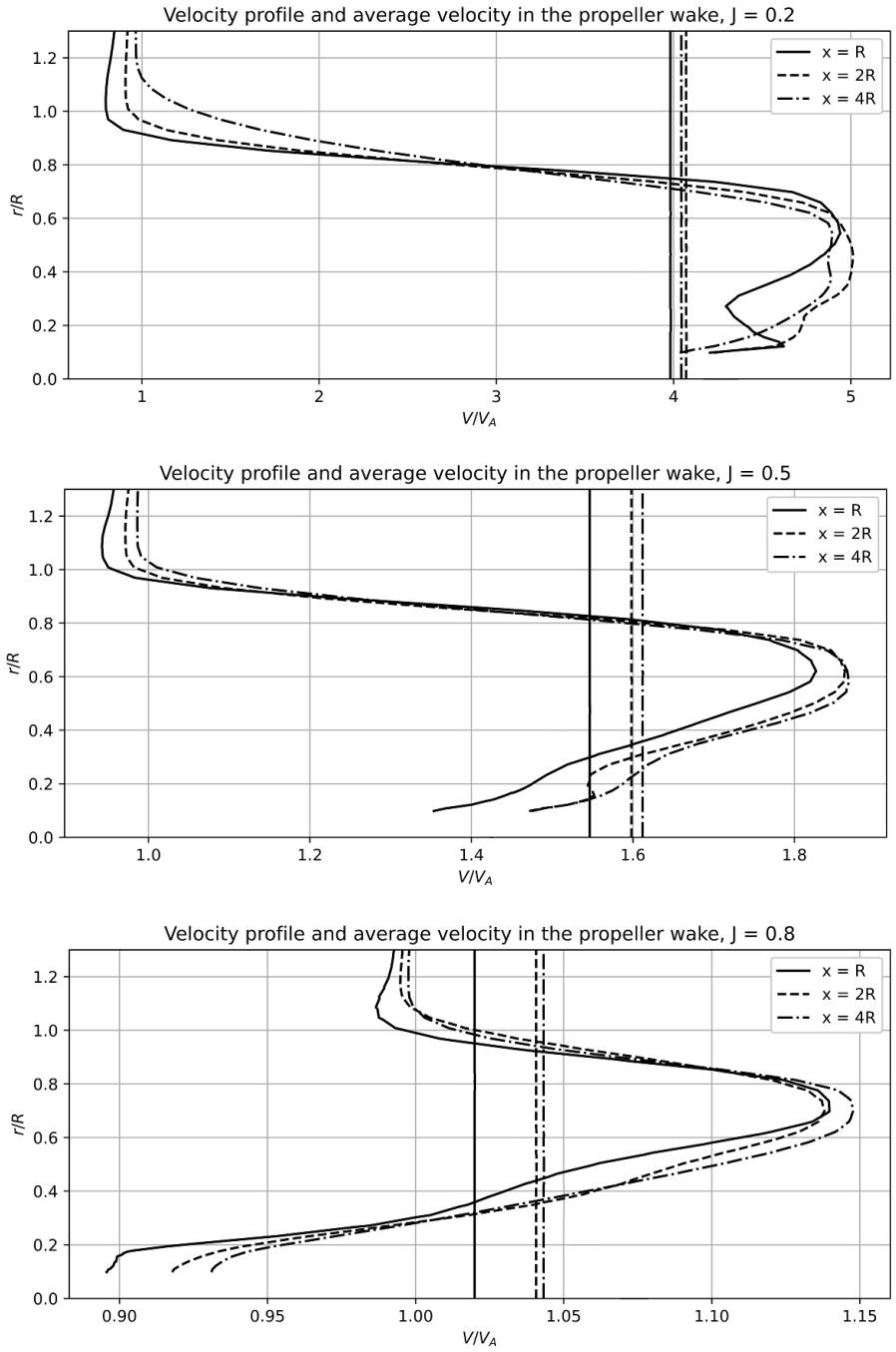

Figure 8 – Open water propeller test in CFD for KVLCC2: normalised velocity profile and average value in the wake of the propeller at three locations aft of the propeller plane (x = R, $2R$, $4R$) for three advance rates J.

Another flow component to be considered is the lateral inflow to the rudder which is hampered by the presence of the hull. This is modelled using a k_H function: the flow straightening factors for the lateral inflow to the rudder. The flow is straightened due to the presence of the hull, $k_H < 1$, however, this is only true in case the ship sails forward. In an astern motion the flow to the rudder is rather curved by the hull or $k_H \to 1$, or even larger than 1. k_H should therefore be expressed as a function of the drift

angle of the ship. Also based on model tests, different flow straightening factors for drift and yaw are required:

$$v_R = k_{Hv}v - k_{Hr}r\frac{L_{PP}}{2} \tag{4.22}$$

The flow straightening factor is smaller for the drift motion, in other words, the flow straightening is more severe when the ship is subjected to drift (a steady condition) compared to yaw (a quasi-steady condition), see for instance Figure 9. Both curves have the same form, but larger values are obtained for the yaw motion.

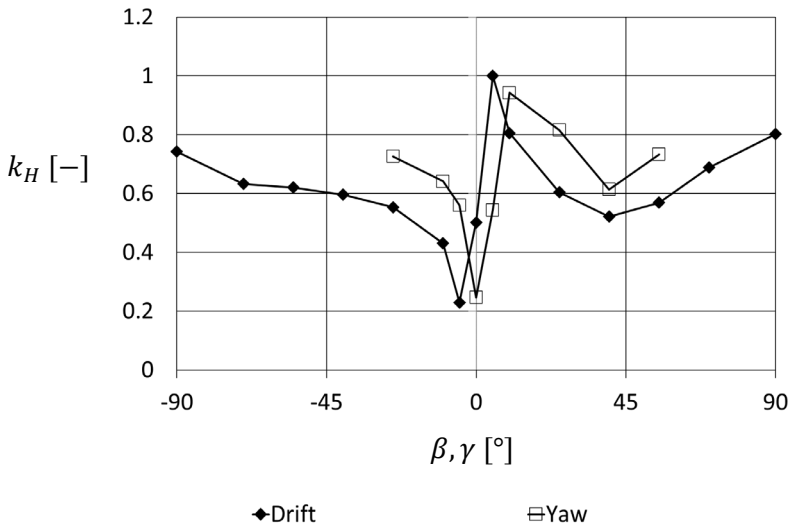

Figure 9 – Flow straightening factors for the lateral rudder force at 50% ukc, first quadrant, KCS

4.4 Longitudinal inflow to the fourth quadrant

4.4.1 First iteration

An independent regression analysis is performed using the longitudinal inflow model mentioned in (4.11) and (4.12) to compute the values of K_m, w_R, k_{Hv} and k_{Hr}. For the wake factor w_R a constant value was used. The results are shown in Figure 10. For reasons of continuity K_m should have the same value for all quadrants, but this seems to be the case if the magnitudes are compared with Figure 5. Also the flow straightening coefficients seem to have a reasonable continuity.

However, the supposedly constant wake factor has a large value in the fourth quadrant and induces a strong discontinuity to the first quadrant. Moreover, the model correlation was mediocre. The latter has several reasons. A first reason is that the theoretical inflow model seems to underpredict the inflow speed in the fourth quadrant. A second important reason is the presence of oscillations in the lateral rudder force of the fourth quadrant. As can be seen in Figure 11 the amplitudes of these oscillations can be significant at large propeller rates, it is however not the aim here to implement an oscillation model.

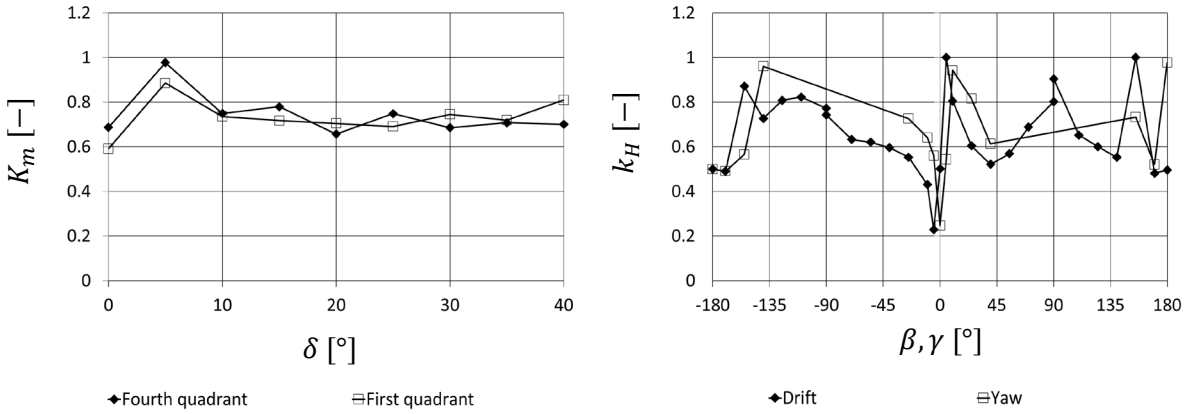

Figure 10 – Propeller jet contraction and flow straightening for the lateral rudder force, 50% ukc, fourth quadrant

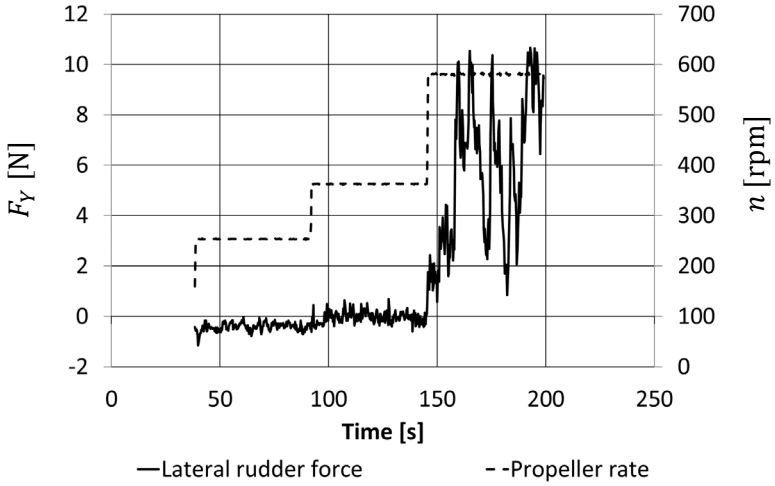

Figure 11 – Evolution of the lateral rudder force, straight line test at -0.35 m/s, different propeller rates, 50% ukc

4.4.2 Vortex ring effect

In the publication of Häusler et al. (2015) the authors describe a novel four quadrant propeller model which computes the outflow of the propeller. Although they use different symbols compared to the present publication, their approximation is based on momentum theory as well and they have thus similar expressions as the ones elaborated in section 4.1. One interesting part, however, is that they state the jet expressions are not valid for:

$$-2 < \frac{v_r}{v_{i0}} < 0 \tag{4.23}$$

with:

- v_r: the inflow to the propeller ($= (1 - w_T)u$ according to the symbols used in this paper);
- v_{i0}: the velocity induced by the propeller at bollard pull conditions (equation (4.15) with $K_m = 1$)

The limits established by equation (4.23) are comparable to the fourth quadrant region, approaching bollard pull conditions (more or less $-25° < \varepsilon^* < 0$) and the authors refer to this interval as the *windmilling region*, but it is actually *vortex ring state* (Johnson, 1980). In this interval momentum theory is invalid because a well-defined slipstream does not exist due to the opposite directions for the flow inside and outside of the slipstream in the far wake (Johnson, 1980). Due to the interaction of the tip vortices with the blades, the flow becomes unsteady and turbulent (Leishman, 2002).

In practice the velocity reaching the rudder is larger than the velocity predicted by momentum theory. Figure 12 shows the correction employed by Häusler et al. (2015), with v_i the induced velocity by the propeller at sailing conditions. Rather than a downward trend between the boundaries of equation (4.23), an uplift is needed for a correct inflow prediction.

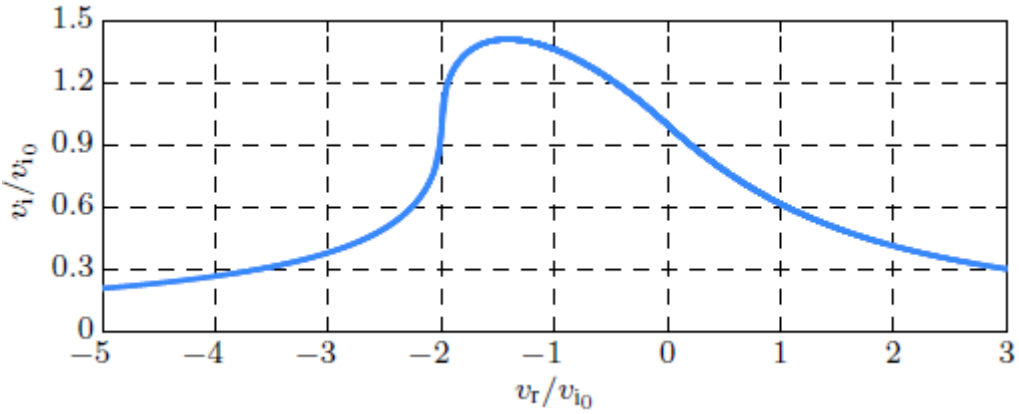

Figure 12 - Velocity ratio plot obtained using the odd square and square root functions. (Häusler et al, 2015)

In the notations used in the present paper, the inflow speed to the rudder due to propeller action in the fourth quadrant can be written as (see the Appendix):

$$u_{RP} = u_{R0} + K_m \left(\sqrt{u_P^2 \left(1 + \left| \frac{8K_T}{\pi J^2} \right| \right)} + u_P \right) \tag{4.24}$$

This expression eventually leads to the fourth quadrant inflow velocity expressions mentioned in section 4.1. The *vortex ring state effect* applied to equation (4.24), implies that the term

$$K_m \left(\sqrt{u_P^2 \left(1 + \left| \frac{8K_T}{\pi J^2} \right| \right)} + u_P \right) \tag{4.25}$$

should be larger than what is predicted by momentum theory. An increase of this term is consequently governed by an increase of K_m. Alternatively the same objective can be attained through a decrease of the wake factor for the thrust in the fourth quadrant, but the latter is mostly zero. For that reason an increase of K_m is expected in the zone depicted by equation (4.23), or in the present paper, it is probable that K_m depends on ε^* in the fourth quadrant.

4.4.3 Application to the KCS

The implementation adds an uplift (or multiplicator) to K_m which is tabulated as a function of ε^*. The multiplicator is equal to 1 in quadrants 1, 2 and 3 and is a regression variable in quadrant 4. The implementation has been tested with the KCS, see Figure 13 for the lateral rudder force of the KCS.

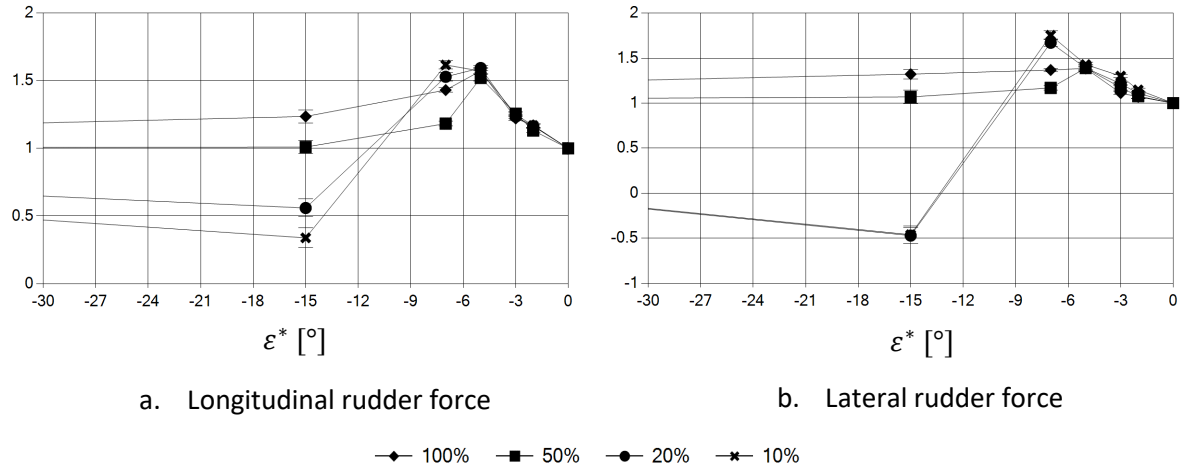

a. Longitudinal rudder force

b. Lateral rudder force

Figure 13 – Uplift (or multiplicator) to K_m in the fourth quadrant, KCS

A better prediction is obtained using the uplift. For smaller propeller rates somewhat more variability in the size of the uplift can be observed, for instance, here even lowering or even opposing the inflow speed. The lowering of the inflow speed is relative, because the total generated inflow speed also becomes smaller when the propeller loading angle becomes more negative. A negative uplift coefficient means that a negative inflow velocity to the rudder is needed sooner than theoretically predicted.

4.5 Longitudinal inflow to the second and third quadrant

Typical for the astern propulsion cases are the significantly lower magnitudes of the measured forces and torque which indicate the dominance of the propeller in the rudder's capabilities. In the third quadrant the same methodology has been applied to determine $K_m(|\delta|), w_R(\varepsilon^*), k_{Hv}(\beta)$ and $k_{Hr}(\gamma)$. For large rudder angles, $K_m(|\delta|)$ has the same magnitude over all quadrants. The flow straightening coefficient for drift has similar magnitudes in the fourth and the third quadrant, but they are not exactly the same. These observations can be put into perspective because the forces acting on the rudder in the third quadrant are significantly smaller compared to the first and the fourth quadrant. The fact that rudder forces measured in the second quadrant are negligible means that the theoretical inflow formula can and should be applied as is for reasons of continuity.

Due to the fact that many parameters are treated as regression coefficients, the regression analysis has become complex and good starting values are needed to avoid parametric drift.

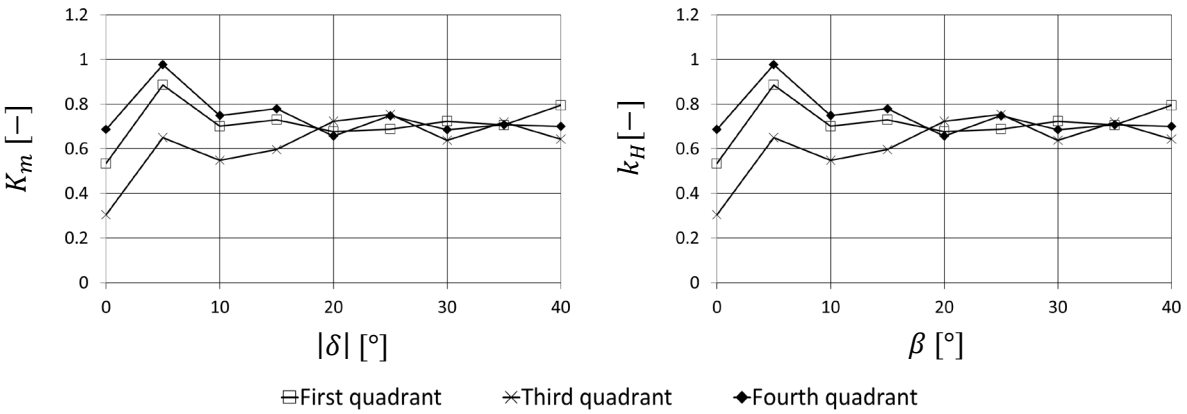

Figure 14 – Propeller jet contraction and flow straightening for the lateral rudder force, 50% ukc, third quadrant

5 Modelling of the rudder torque

5.1 Model of the centre of pressure

One of the main difficulties in prediction the torque of the rudder around its shaft, see equation (2.9), is the sign change of the centre of pressure (the application point of the lateral rudder force), which tends to move forward with propeller loading, as noted by Molland & Turnock (2007).

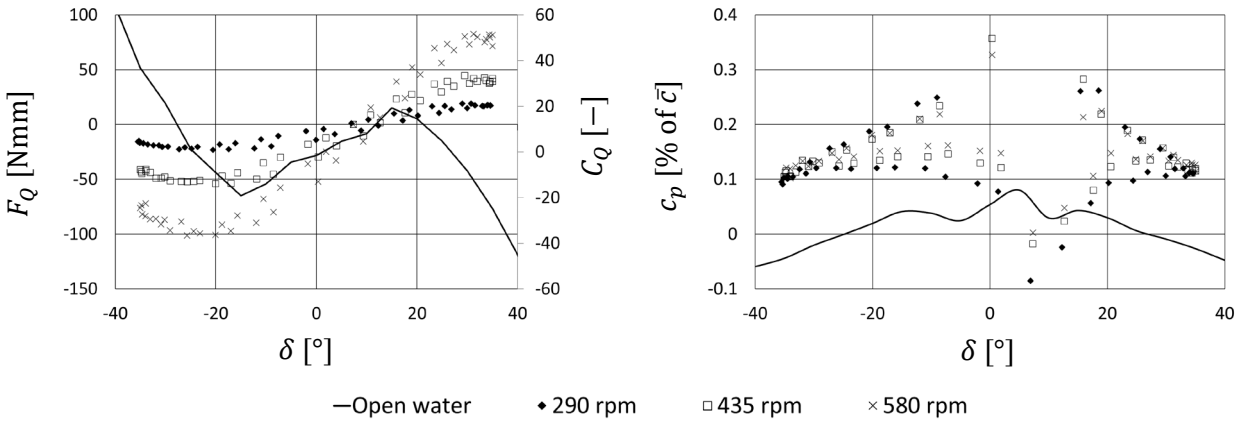

Figure 15 – Measured rudder torque in open water conditions, 50% ukc, KCS

This problem has been visualised for the bollard pull condition in Figure 15. The tests presented in this graph were carried out with a harmonically varying rudder angle for a constant propeller rate, which explains the hysteresis on the figures. At large rudder angles the rudder torque in bollard pull conditions clearly has a different sign compared to the open water condition. In general the centre of pressure is shifted forward, which causes the sign change of the torque. Observe that the scatter in the centre of pressure near 5° is due to the fact that the lateral rudder force is almost zero. Disregarding this scatter it seems that the centre of pressure in bollard pull conditions is more or less parallel with the open water curve. This suggest that the centre of pressure can be written as:

$$c_P = c_{P,\text{open water}} + c_{P,\text{bollard pull}} \tag{5.1}$$

The above has been extended by the following model, applicable to all quadrants:

$$c_P = c_{P,\text{open water}} + c_P(\varepsilon^*) \tag{5.2}$$

The 15 values of $c_P(\varepsilon^*)$ have been plotted in Figure 16. In the first and fourth quadrant the centre of pressure tends to move more forward while ε^* becomes more negative. A local minimum is observed near bollard pull. When the propeller is stopped large values are obtained, but these are due to the smaller to negligible lateral rudder forces.

Please observe that there may be scaling issues because the backward movement of the centre of pressure with respect to rudder angle for the ship model is higher than that for a real ship due to different Reynolds numbers.

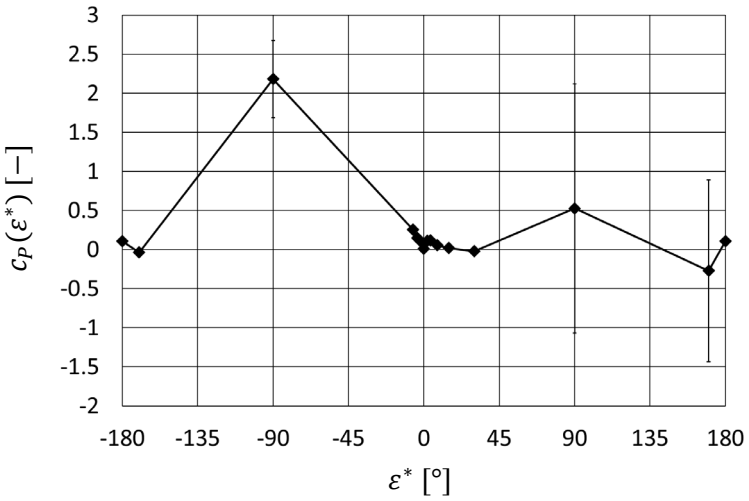

Figure 16 – Change in the centre of pressure due to propeller loading, 50% ukc

5.2 Influence of drift and yaw on the rudder torque

Using the above model the prediction accuracy is not yet acceptable. The differences between the modelled and measured rudder torques were investigated and it seems that the errors increase with increasing drift or yaw motion. Although the latter should be included in the lateral rudder force, the effect on the rudder torque is not sufficiently well predicted.

To cover this issue, the rudder is considered to be a small ship form subjected to drift and yaw motion, and similarly to the yaw moment of the ship, the rudder torque can be modelled by:

$$F_Q = F_Y \left(c_{p,\text{open water}} + c_p(\varepsilon^*)\right) \bar{c} + \frac{\rho}{2} A_R \bar{c} (u^2 + v^2) F_Q(\beta) + \frac{\rho}{2} A_R \bar{c} \left(u^2 + \left(\frac{rL}{2}\right)^2\right) F_Q(\gamma) \tag{5.3}$$

Mind that in the above equation $F_Q(\beta)$ and $F_Q(\gamma)$ are expressed with the ship's speed and not with the inflow speed of the rudder. These two functions are represented in Figure 17. As can be seen their value is limited for small angles, but significant for larger angles. The forward movement of the centre of pressure in the first and fourth quadrant seems to diminish with decreasing under keel clearance,

but the drift and yaw influence becomes more significant with decreasing under keel clearance. Adding the two functions $F_Q(\beta), F_Q(\gamma)$ leads to an acceptable prediction accuracy for simulation purposes.

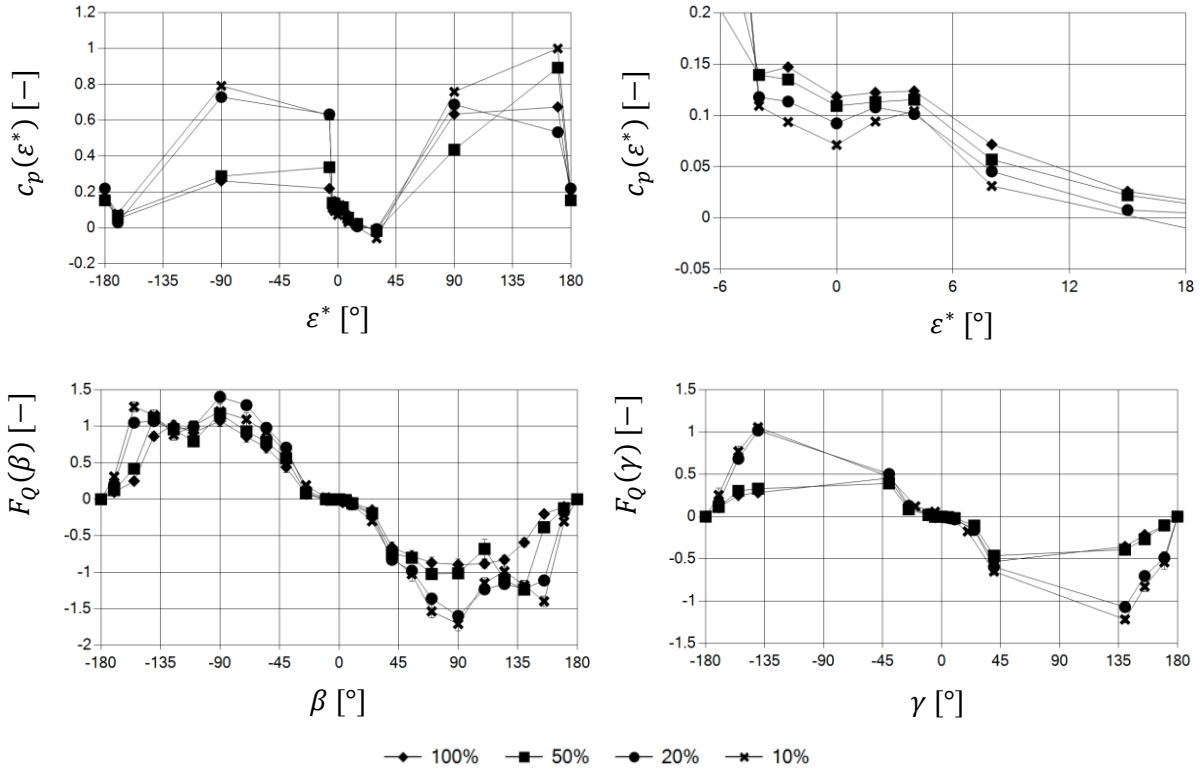

Figure 17 – Rudder torque coefficients for all ukc

5.3 Steering engine

5.3.1 Literature review

The main advantage of having the rudder torque modelled is the possibility to implement a steering engine to steer the rudder angle and to investigate possible effects of the under keel clearance or machine failure on the rudder rate, analogously as for the propeller shaft torque. To this end a short internet search has been conducted in order to gain insight in the behaviour of the steering gear. However the available information is rather scarce and the presented information is based on classification societies and engine manufacturers.

Steering engines can be classified into three types (China Classification Society, 2018):

- Piston type;
- Ram type;
- Rotatory vane type.

An example of each type is shown in Figure 18. Both the piston and ram type engine work based on hydraulic pistons. Due to the simplicity, but limited power, the first is more used in smaller ships (up to 30,000 DWT according to MacGregor (2018)), while the second can be used in larger ships as well, as is the case for the rotatory vane type.

The piston type rudder is steered by changing the pressure in both pistons. In the ram type "*there are four hydraulic cylinders attached to the two arms of the actuator disc, on both sides. These cylinders are directly coupled to electrically driven hydraulic pumps which generate hydraulic pressure through pipes. This hydraulic pressure field present in the pumps imparts motion to the hydraulic cylinders, which in turn corresponds with the actuator to act upon the rudder stock. In the rotary vane steering gear, there is a fixed housing in which two vanes rotate. The housing along with the vanes form four chambers. The physics behind its operation is similar to the ram type.*" (direct citation from Marine Insight (2018)).

The delivered maximal steering torque ranges from 24 kNm to 950 kNm for the piston type (MacGregor, 2018) and from 430 kNm to 6,565 kNm for the rotatory vane system (RollsRoyce, 2018). These values are mostly valid at a rudder angle of 35°.

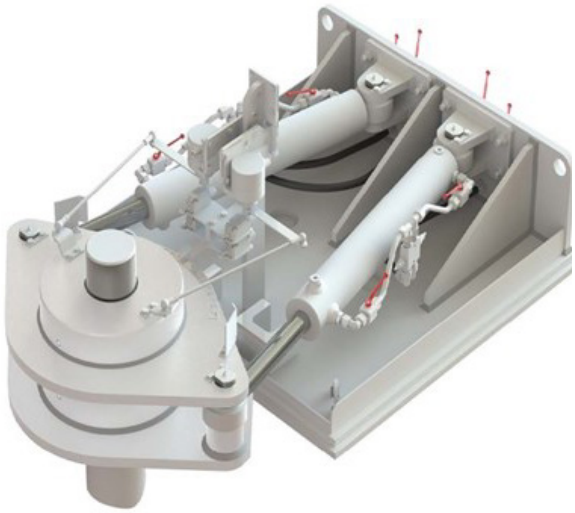

a. Piston type (MacGregor, 2018)

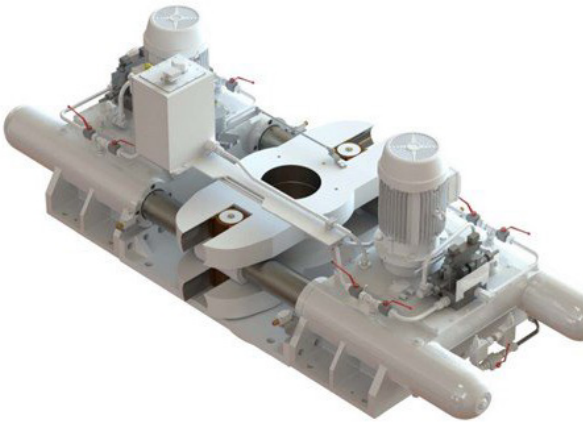

b. Ram Type (MacGregor, 2018)

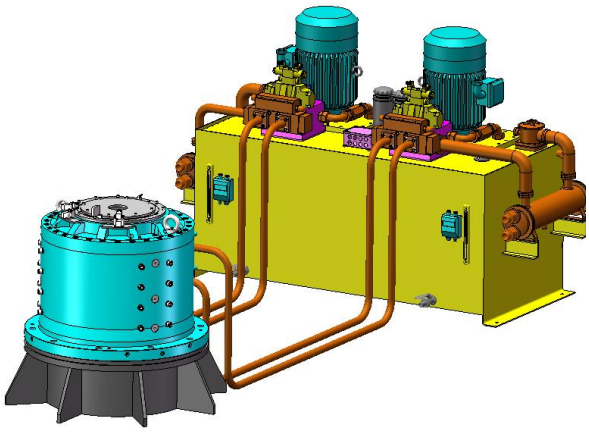

c. Rotatory vane (with energy supply) (Dieselship, 2018)

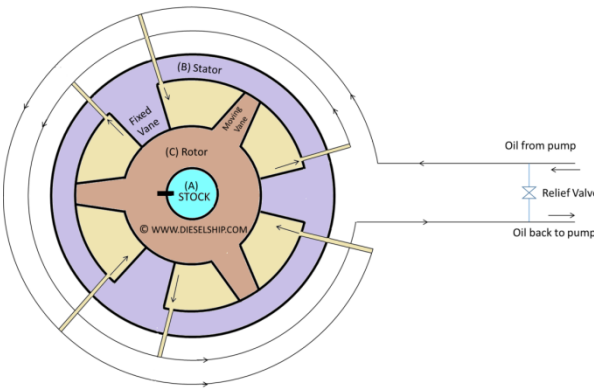

d. Rotatory vane: working principle. (Dieselship, 2018)

Figure 18 – Types of steering gear

At present no information has been found on ships equipped with a specific engine. Classification societies give empirical formulae to compute the necessary torque so that the ship can meet the IMO regulations:

- At full speed and at deepest draft the ship has to be able to move its rudder from 35° on one side to 35° on the other side;
- Under the same conditions the movement from 35° on either side to 30° on the other side has to be performed in not more than 28 s.

For instance the China Classification Society gives the following formulae to compute the torque for each type of rudder:

- Ram type:

$$M_1 = \frac{\pi D_1^2 R_1 \Delta P \eta_1 \cos^2 \alpha}{4} 10^{-6} kNm \tag{5.4}$$

- Piston type:

$$M_2 = \frac{\pi (2D_2^2 - d_2^2) R_2 \Delta P \eta_2 \cos \alpha}{4} 10^{-6} kNm \tag{5.5}$$

- Rotatory vane type:

$$M_3 = 0.125 i H (D_3^2 - d_3^2) \Delta P \eta_3 10^{-6} kNm \tag{5.6}$$

see China Classification Society (2018) for more information on the symbols. Similar formulae are available at ABS or DNV-GL. The above formulae are mainly based on the size of the engine, the efficiency and the rudder angle α. The latter indicates that for both the ram and piston type the torque efficiency decreases with increasing rudder angle, while the rotatory vane type can deliver a constant torque. Probably for this reason the rotatory vane type is mostly used in larger vessels.

5.3.2 Implementation

When a new rudder angle is desired the steering gear will deliver the necessary torque Q_{SG} so that the rudder is accelerated as follows:

$$\ddot{\delta}_R = \frac{Q_{SG} - F_Q}{I_{ZZ,\text{rudder}}} \tag{5.7}$$

The steering torque is either dependent of the present rudder angle (piston and ram type) or constant (rotatory vane type). Presently both the piston and rotatory vane type have been implemented. Provided that the maximal torque $Q_{SG,\max}$ is given in the equipment file:

$$Q_{SG} = Q_{SG,\max} \cos \delta_R \tag{5.8}$$

for the piston type and

$$Q_{SG} = Q_{SG,\max} \tag{5.9}$$

for the rotatory vane type. With a change of variables ($a_1 = \delta_R, a_2 = \dot{\delta}_R$), equation (5.7) is converted in two first-order ordinary differential equations (ODE) ($\dot{a}_1 = a_2$ and $\dot{a}_2 = \ddot{\delta}_R$) with initial values $a_1(t_0) = \delta_R(t_0)$ and $a_2(t_0) = \dot{\delta}_R(t_0)$ that can be solved with any standard ODE solver.

The rudder velocity is limited by the maximally available rudder speed, if needed limited by prescribed failures, like no piston action, thus constant rudder angle or only half of the pistons work, thus half speed of the rudder. If the oil pressure disappears the rudder angle will be determined by the free running condition:

$$\ddot{\delta}_R = \frac{-F_Q}{I_{ZZ,\text{rudder}}} \tag{5.10}$$

In other words the rudder angle will correspond to the position which minimises the rudder torque.

5.3.3 Working example for the KCS

The above has been tested with the KCS. Additional data were needed such as the moment of inertia about the rudder stock:

- Inertia radius of the rudder about the rudder stock r_{stock} = 1.625 m;
- Volume of the rudder: 36.64 m³.

The moment of inertia about the rudder stock is then:

$$I_{ZZ,\text{rudder}} = m_{\text{rudder}} r_{\text{stock}}^2 \tag{5.11}$$

The mass of the rudder has been estimated as 36.64 ton. This is based on the observation that the rudder volume has the same order of magnitude as the rudder mass (ρ_{avg}=1000 kg/m³) for most rudders, which gives for the KCS $I_{ZZ,\text{rudder}}$ = 96,748 kgm².

The maximal steering torque has been estimated for the KCS as 1000 kNm as this value seems to be typical for midsize ships. In reality a steering engine should be designed and optimised considering the real weight and (added) mass distribution of the rudder and taking account of the friction torque due to the bearing. However, such detailed computations fall outside of the scope of the present paper. The simulation in Figure 19a reveals indeed that the rudder movement does not present any issue with such torque, compared to when only 100 kNm would be available.

An example of failure of the oil pressure is shown in Figure 19b. The ship has a rudder angle of -10° when oil pressure is lost. The steering gear directs the rudder towards an average angle of +7.5° which minimizes the rudder torque.

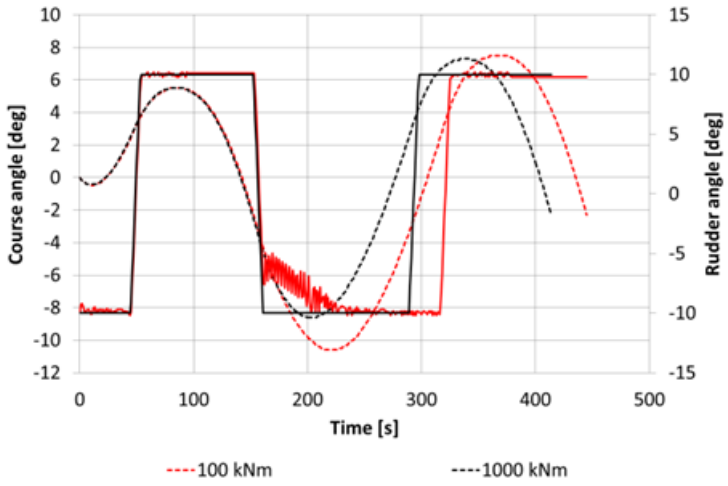

a. 10/2.5 zigzag test: influence of maximal available steering torque

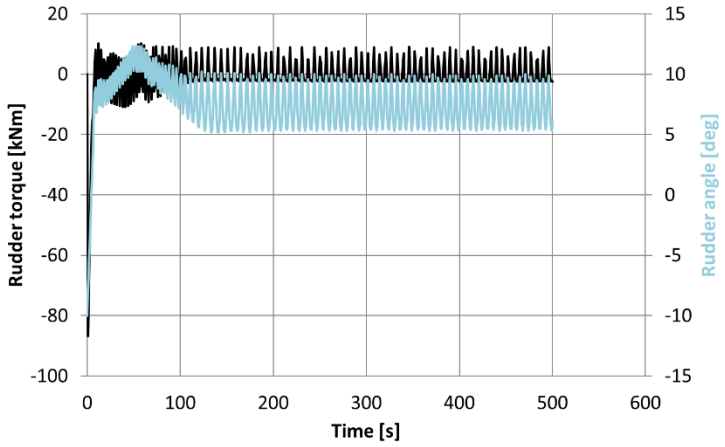

b. Steering without available oil pressure, starting at -10° rudder angle

Figure 19 – Examples of steering torque dependent simulations, 100% ukc, approach conditions: 9 knots at 43 rpm.

5.4 Remark

The mathematical model of the rudder torque was also tested on other ships, however the results were disappointing. Based on other ships, it seemed better to model c_p as a function of the inflow angle (for the lateral rudder force) and to add a propulsion dependent function:

$$F_Q = F_Y\left(c_{p,\text{open water}} + c_p(\alpha)\right)\bar{c} + \frac{\rho}{2}A_R\bar{c}(u^2+v^2)F_Q(\beta) + \frac{\rho}{2}A_R\bar{c}\left(u^2+\left(\frac{rL}{2}\right)^2\right)F_Q(\gamma) + \rho n^2 D_P^5 F_Q(\varepsilon^*) \quad (5.12)$$

With this formulation a much better accuracy is achieved for the other ships, while maintaining a similar accuracy for the KCS. In the future, additional computations will be carried using other ships which will possibly lead to a better prediction formula.

6 Validation

A two-step validation has been performed. Firstly, an overall assessment between measurements and the mathematical model has been performed for all tests. The resulting trend lines and correlation coefficients are presented in in Table 2 and Table 3. The agreement is quite well for the rudder force components, however, in general a slight underprediction is still seen, mainly due to the underprediction in astern motion. The rudder torque prediction is usable, but should be further enhanced.

Secondly, the modelled rudder forces were compared with the results of free running model tests. An example is shown in Figure 20. A good accuracy is obtained, however, with a slight underprediction of the lateral rudder force in this specific test.

Table 2 – Comparison between measured and modelled rudder forces

ukc	Longitudinal force [N]	Lateral force [N]
100%	$F_{X,\mathrm{mod}} = 0.9485F_{X,\mathrm{meas}} - 0.0217$ $R^2 = 0.9416$	$F_{Y,\mathrm{mod}} = 0.9562F_{Y,\mathrm{meas}} + 0.0171$ $R^2 = 0.9509$
50%	$F_{X,\mathrm{mod}} = 0.9340F_{X,\mathrm{meas}} - 0.0372$ $R^2 = 0.9148$	$F_{Y,\mathrm{mod}} = 0.9477F_{Y,\mathrm{meas}} + 0.0022$ $R^2 = 0.9454$
20%	$F_{X,\mathrm{mod}} = 0.9430F_{X,\mathrm{meas}} - 0.0288$ $R^2 = 0.9338$	$F_{Y,\mathrm{mod}} = 0.9422F_{Y,\mathrm{meas}} - 0.0097$ $R^2 = 0.9427$
10%	$F_{X,\mathrm{mod}} = 0.9066F_{X,\mathrm{meas}} - 0.0421$ $R^2 = 0.9112$	$F_{Y,\mathrm{mod}} = 0.9028F_{Y,\mathrm{meas}} + 0.006$ $R^2 = 0.9127$

Table 3 – Comparison between measured and modelled rudder torque

ukc	Rudder torque [Nmm]
100%	$F_{Q,\mathrm{mod}} = 0.7508F_{\mathrm{Q,meas}} - 1.0094$ $R^2 = 0.7600$
50%	$F_{Q,\mathrm{mod}} = 0.6736F_{\mathrm{Q,meas}} - 0.9958$ $R^2 = 0.6751$
20%	$F_{Q,\mathrm{mod}} = 0.6165F_{\mathrm{Q,meas}} - 1.4482$ $R^2 = 0.6143$
10%	$F_{Q,\mathrm{mod}} = 0.6540F_{\mathrm{Q,meas}} - 1.2043$ $R^2 = 0.6594$

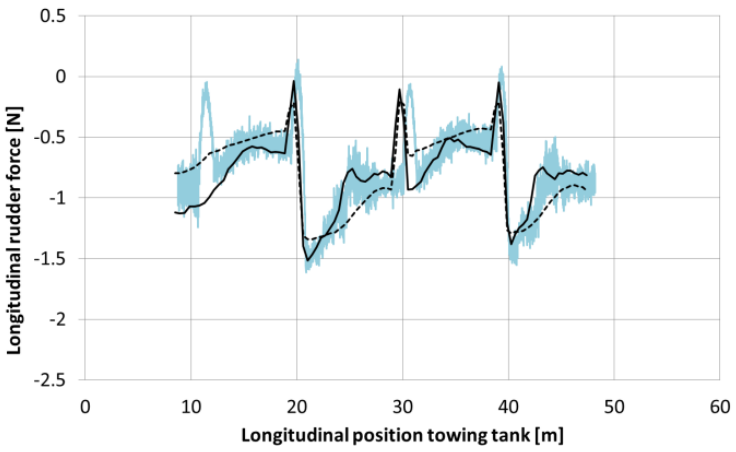

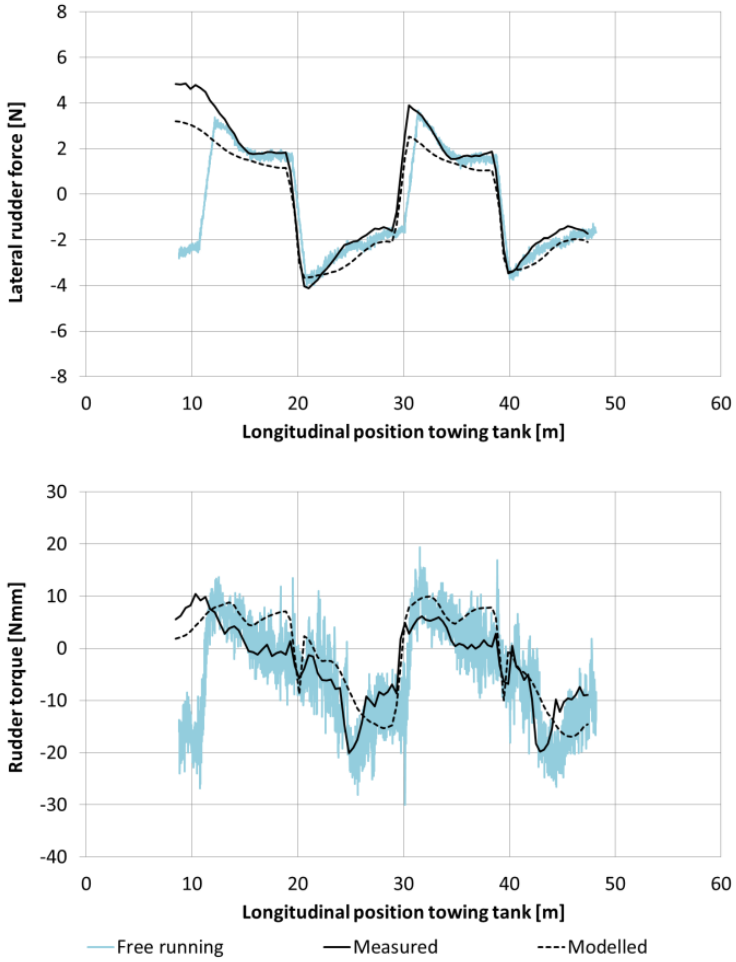

Figure 20 – Comparison between the modelled rudder forces and measured ones in a -20/5 free running tests, 50% ukc, full scale approach conditions: 9 knots at 43 rpm. The line 'Measured' represents a measurement of a captive model tests which was executed afterwards mimicking the track of the free running test.

7 Conclusions and outlook

This paper introduces a physics-based mathematical model for forces and torque acting on a rudder in hull-propeller-rudder configuration. The novelty resides in the application of momentum theory in a four-quadrant approach with full continuity for harbour manoeuvres. As momentum theory lacks validity over the full four quadrant range a correction is proposed in the fourth quadrant, based on helicopter theory. Additionally a model for the steering torque is introduced which enables one to study the effect of steering engine failures when manoeuvring in harbour areas.

The new mathematical model has been applied to a number of sea-going and inland ships already, but here the well-known benchmark ship KCS is used as illustrative example for different shallow water depths. For most ships, including the KCS, the improved mathematical model results in a better prediction capability of the rudder forces. The downside is that the number of coefficients to be determined and the relation between them forces the user to have a significant amount of tests at his disposal and a critical eye on the regression process.

In the future, numerical methods will be used to quantify the flow field due to interaction between hull, propeller and rudder and to possibly enhance the present formulation. More research will be dedicated to the steering torque as well and its behaviour during standard manoeuvres and harbour manoeuvres.

8 References

Calcagni, D., Salvatore, F., Dubbioso, G. and Muscari, R., 2017, "A Generalised Unsteady Hybrid DES/BEM Methodology Applied to Propeller-Rudder Flow Simulation", MARINE 2017, pp. 377–392.

Delefortrie, G., Geerts, S., Vantorre, M., 2016. "The towing tank for manoeuvres in shallow water", Proceedings of the 4th International Conference on Ship Manoeuvring in Shallow and Confined Water with Special Focus on Ship Bottom Interaction, Hamburg, Germany, 23 to 25 May 2016 (4th MASHCON). pp. 226-235

Delefortrie, G., Eloot, K., Van Hoydonck, W., 2020, "EFD based submissions for the shallow water cases of SIMMAN 2020". Preprint submitted to the SIMMAN workshop, www.simman2019.kr

Fukui, Y., 2012, "A Study on Interaction Coefficients between Hull and Rudder in Maneuvering Model Using CFD", MARSIM 2012, Singapore.

Hasanvand, A., Hajivand, A. and Ale ali, N., 2019, "Investigating the Effect of Rudder Profile on 6DOF Ship Turning Performance", Applied Ocean Research, Vol. 92, pp. 1–21

Häusler, A.J.; Saccon, A.; Hauser, J.; Pascoal, A.M.; Aguiar, A.P. (2015). A Novel Four-Quadrant Propeller Model. Fourth International Symposium on Marine Propulsors. Austin, Texas, USA, June 2015.

Johnson, W. (1980). Helicopter theory. Dover Publications: New York. ISBN 0-486-68230-7. 1089 pp.

Leishman, J.G. (2002). Principles of helicopter aerodynamics. Cambridge University Press: Cambridge, UK. ISBN 0-521-52396-6. 496 pp.

Kaidi, S., Smaoui, H. and Sergent, P., 2018, "CFD Investigation of Mutual Interaction between Hull, Propellers, and Rudders for an Inland Container Ship in Deep, Very Deep, Shallow, and Very Shallow Waters", Journal of Waterway, Port, Coastal and Ocean Engineering, Vol. 144, No.6.

Mofidi, A., Martin, J. E. and Carrica, P. M., 2018, "Propeller/Rudder Interaction with Direct and Coupled CFD/Potential Flow Propeller Approaches, and Application to a Zigzag Manoeuvre", Ship Technology Research, Vol. 65, No.1, pp. 10–31.

Molland, A.F.; Turnock, S.R. (2007). Marine rudders and control surfaces: principles, data, design and applications. Elsevier: Amsterdam. ISBN 978-0-75-066944-3. xvii, 420 pp.

Shen, Y. and Hughes, M., 2012, "Effective Inflow Velocity for Rudder Calculations", International Shipbuilding Progress, Vol. 59, pp. 107–127

Su, Y. and Kinnas, S. A., 2018, "A Time-Accurate BEM/RANS Interactive Method for Predicting Propeller Performance Considering Unsteady Hull/Propeller/Rudder Interaction", 32nd Symposium on Naval Hydrodynamics , Hamburg, Germany, pp. 5–10.

Van Hoydonck, W., Delefortrie, G., De Maerschalck, B. and Vantorre, M., 2018, "Open-Water Rudder Tests Using CFD", 32nd Symposium on Naval Hydrodynamics, Hamburg, Germany, pp. 1–14.

Villa, D., Viviani, M., Tani, G., Gaggero, S., Bruzzone, D. and Podenzana, C. B., 2018, "Numerical Evaluation of Rudder Performance Behind a Propeller in Bollard Pull Condition", Journal of Marine Science and Application, Vol. 17, No.2, pp. 153–164.

Yang, H., Lee, J. and Kim, K., 2015, "Numerical and Experimental Study on the Rudder Force of a Twisted Rudder", MARSIM 2015, Newcastle, UK, 11 pp.

Yasukawa, H. and Yoshimura, Y., 2015, "Introduction of MMG Standard Method for Ship Maneuvering Predictions", Journal of Marine Science and Technology, Vol. 20, No.1, pp. 37–52.

Websites accessed in 2018:

China Classification Society (2018). www.ccs.org.cn

Dieselship (2018). www.dieselship.com

MacGregor (2018). www.macgregor.com

Marine Insight (2018). www.marineinsight.com

Rolls Royce (2018). https://www.rolls-royce.com

9 Appendix 1: Derivation of the expressions for longitudinal inflow to the rudder

9.1 First quadrant

9.1.1 Formulation

The inflow velocity to a rudder located behind a propeller can be derived from momentum theory:

$$u_{RP} = u_{R0} + K_m u_p \left(\sqrt{1 + \frac{8K_T}{\pi J^2}} - 1 \right) \tag{9.1}$$

Because only a part η of the rudder is located in the propeller jet, the average inflow to the rudder is:

$$u_R = \sqrt{\eta u_{RP}^2 + (1-\eta) u_{R0}^2} \tag{9.2}$$

It can be proven that:

$$\frac{8K_T}{\pi J^2} = \frac{C_T}{\sin^2 \varepsilon} \tag{9.3}$$

In this way (9.2) can be reformulated as:

$$
\begin{aligned}
u_R &= \sqrt{\eta\left[u_{R0} + K_m u_p\left(\sqrt{1+\frac{C_T}{\sin^2\varepsilon}}-1\right)\right]^2 + (1-\eta)u_{R0}^2} \\
u_R &= \sqrt{\eta\left[(1-w_R)u + (1-w_T)K_m u\left(\sqrt{\frac{\sin^2\varepsilon+C_T}{\sin^2\varepsilon}}-1\right)\right]^2 + (1-\eta)[(1-w_R)u]^2} \\
u_R &= (1-w_R)u\sqrt{\eta\left[1+\frac{(1-w_T)}{(1-w_R)}\frac{K_m}{\sin\varepsilon}\left(\sqrt{\sin^2\varepsilon+C_T}-\sin\varepsilon\right)\right]^2 + (1-\eta)}
\end{aligned}
\tag{9.4}
$$

The last step is only valid for $w_R < 1$. Introducing the parameter

$$
\zeta = \frac{1-w_R}{1-w_T} \tag{9.5}
$$

(9.4) can be further transformed to

$$
\begin{aligned}
u_R &= (1-w_R)u\sqrt{\frac{\eta}{\sin^2\varepsilon}\left[\sin\varepsilon + \frac{K_m}{\zeta}\left(\sqrt{\sin^2\varepsilon+C_T}-\sin\varepsilon\right)\right]^2 + (1-\eta)} \\
u_R &= (1-w_R)\frac{u}{\sin\varepsilon}\sqrt{\eta\left[\left(1-\frac{K_m}{\zeta}\right)\sin\varepsilon + \frac{K_m}{\zeta}\left(\sqrt{\sin^2\varepsilon+C_T}\right)\right]^2 + (1-\eta)\sin^2\varepsilon}
\end{aligned}
\tag{9.6}
$$

Considering the fact that

$$
\frac{u}{\sin\varepsilon} = \frac{\sqrt{(0.7\pi n D_P)^2 + u_P^2}}{1-w_T} \tag{9.7}
$$

which leads to

$$
u_R = \zeta\sqrt{\left[\eta\left[\left(1-\frac{K_m}{\zeta}\right)\sin\varepsilon + \frac{K_m}{\zeta}\left(\sqrt{\sin^2\varepsilon+C_T}\right)\right]^2 + (1-\eta)\sin^2\varepsilon\right][(0.7\pi n D_P)^2 + [(1-w_T)u]^2]} \tag{9.8}
$$

9.1.2 Limits

In bollard pull condition, with $u = 0$ and $\sin\varepsilon = 0$, (9.8) can be rewritten as:

$$
\begin{aligned}
u_R &= \zeta\sqrt{\eta\left[\frac{K_m}{\zeta}\sqrt{C_T}\right]^2(0.7\pi n D_P)^2} \\
u_R &= \zeta 0.7\pi n D_P\frac{K_m}{\zeta}\sqrt{\eta C_T} \\
u_R &= 0.7\pi n D_P K_m\sqrt{\eta C_T}
\end{aligned}
\tag{9.9}
$$

The inflow does not depend on any wake factor, the only possible variable to determine the inflow is K_m.

If the propeller is not turning, with $n = 0$, and $\sin\varepsilon = 1$, (9.8) can be rewritten as:

$$
\begin{aligned}
u_R &= \zeta(1-w_T)u\sqrt{\left[\eta\left[\left(1-\tfrac{K_m}{\zeta}\right)+\tfrac{K_m}{\zeta}\left(\sqrt{1+\lim_{\varepsilon\to\frac{\pi}{2}} C_T}\right)\right]^2+(1-\eta)\right]} \\
u_R &= (1-w_R)u\sqrt{\left[\eta\left[\left(1-\tfrac{K_m}{\zeta}\right)+\tfrac{K_m}{\zeta}\left(\sqrt{1+0}\right)\right]^2+(1-\eta)\right]} \\
u_R &= (1-w_R)u
\end{aligned}
\tag{9.10}
$$

which is a logical result. $\lim_{\varepsilon\to\frac{\pi}{2}} C_T$ has to be equal to zero, but in practice this is not the case due to the own resistance of the propeller. Nevertheless it should be assumed here because of (9.3):

$$
\lim_{J\to\infty}\frac{8K_T}{\pi J^2}=0=\lim_{\varepsilon\to\frac{\pi}{2}}\frac{C_T}{\sin^2\varepsilon} \tag{9.11}
$$

9.2 Second quadrant

9.2.1 Formulation

In the second quadrant the inflow speed is given by

$$
u_{RP}=u_{R0}-(1-K_m)u_p\left(\sqrt{1+\left|\frac{8K_T}{\pi J^2}\right|}-1\right) \tag{9.12}
$$

Considering $u_P=(1-w_T)u$ this can be rewritten as:

$$
u_{RP}=u\left[(1-w_R)-(1-K_m)(1-w_T)\left(\sqrt{1+\left|\frac{8K_T}{\pi J^2}\right|}-1\right)\right] \tag{9.13}
$$

With equations (9.3) and (9.5) the above formula can be transformed as follows:

$$
\begin{aligned}
u_{RP} &= u\left[(1-w_R)-(1-w_T)\tfrac{(1-K_m)}{\sin\varepsilon}\left(\sqrt{\sin^2\varepsilon+|C_T|}-\sin\varepsilon\right)\right] \\
u_{RP} &= u\left[(1-w_R)\tfrac{\sin\varepsilon}{\sin\varepsilon}-\tfrac{(1-w_R)}{\zeta}\tfrac{(1-K_m)}{\sin\varepsilon}\left(\sqrt{\sin^2\varepsilon+|C_T|}-\sin\varepsilon\right)\right] \\
u_{RP} &= (1-w_R)\tfrac{u}{\sin\varepsilon}\left[\left(1+\tfrac{1-K_m}{\zeta}\right)\sin\varepsilon-\tfrac{1-K_m}{\zeta}\sqrt{\sin^2\varepsilon+|C_T|}\right]
\end{aligned}
\tag{9.14}
$$

In which (9.7) can be substituted:

$$
\begin{aligned}
u_{RP} &= \zeta\sqrt{(0.7\pi nD_P)^2+u_P^2}\left[\left(1+\tfrac{1-K_m}{\zeta}\right)\sin\varepsilon-\tfrac{1-K_m}{\zeta}\sqrt{\sin^2\varepsilon+|C_T|}\right] \\
u_{RP} &= \left[(\zeta+1-K_m)\sin\varepsilon-(1-K_m)\sqrt{\sin^2\varepsilon+|C_T|}\right]\sqrt{[(0.7\pi nD_P)^2+[(1-w_T)u]^2]}
\end{aligned}
\tag{9.15}
$$

The sign of u_{RP} is not always positive, which is important for the computation of a weighted average:

$$
u_{RP}=\left[(\zeta+1-K_m)\sin\varepsilon-(1-K_m)\sqrt{\sin^2\varepsilon+|C_T|}\right]\sqrt{[(0.7\pi nD_P)^2+[(1-w_T)u]^2]} \tag{9.16}
$$

$$
\geq 0 \qquad\qquad \leq 0 \qquad\qquad \geq 0
$$

u_{RP} is only positive if:

$$\begin{aligned} u_{RP} &\geq 0 \\ &\Leftrightarrow (\zeta + 1 - K_m)\sin\varepsilon \geq (1 - K_m)\sqrt{\sin^2\varepsilon + |C_T|} \\ &\Leftrightarrow \sin\varepsilon \geq (1 - K_m)\sqrt{\frac{|C_T|}{\zeta[\zeta + 2(1 - K_m)]}} > 0 \end{aligned} \tag{9.17}$$

A sign change of u_{RP} is probable, because the right hand side of the equation is strictly positive and $\sin\varepsilon$ turns zero in bollard pull conditions. The weighted rudder inflow velocity depends on the sign of u_{RP}, which will change at sufficiently large propeller rates:

$$\begin{aligned} u_R &= \text{sign}(u_{RP})\sqrt{\eta u_{RP}^2 + \text{sign}(u_{RP})(1 - \eta)u_{R0}^2}; \eta u_{RP}^2 \geq (1 - \eta)u_{R0}^2 \\ u_R &= \sqrt{\text{sign}(u_{RP})\eta u_{RP}^2 + (1 - \eta)u_{R0}^2}; \eta u_{RP}^2 < (1 - \eta)u_{R0}^2 \end{aligned} \tag{9.18}$$

This is logical, because at a certain point the negative speed of the propeller dominates the positive speed of the ship. The propeller speed is dominant when:

$$\begin{aligned} \eta u_{RP}^2 &\geq (1 - \eta)u_{R0}^2 \\ &\Leftrightarrow \left[\frac{u}{\sin\varepsilon}\left[\left(1 + \frac{1 - K_m}{\zeta}\right)\sin\varepsilon - \frac{1 - K_m}{\zeta}\sqrt{\sin^2\varepsilon + |C_T|}\right]\right]^2 \geq \frac{1 - \eta}{\eta}u^2 \\ &\Leftrightarrow \left|(\zeta + 1 - K_m)\sin\varepsilon - (1 - K_m)\sqrt{\sin^2\varepsilon + |C_T|}\right| \geq \zeta\sqrt{\frac{1 - \eta}{\eta}}|\sin\varepsilon| \end{aligned} \tag{9.19}$$

In case there is no propeller action, with the assumption $C_T = 0$, the above condition simplifies to:

$$\begin{aligned} |(\zeta + 1 - K_m)\sin\varepsilon - (1 - K_m)\sin\varepsilon| &\geq \zeta\sqrt{\frac{1 - \eta}{\eta}}|\sin\varepsilon| \\ \Leftrightarrow \quad 1 &\geq \sqrt{\frac{1 - \eta}{\eta}} \\ \Leftrightarrow \quad \eta &\geq 0.5 \end{aligned} \tag{9.20}$$

While in bollard pull conditions:

$$\left|(1 - K_m)\sqrt{|C_T|}\right| \geq 0 \tag{9.21}$$

The latter is always satisfied. The former is also satisfied for most realistic rudder setups, which indicates that for $\eta \geq 0.5$ two sign changes occur. The first equation of (9.18) can be written as:

$$\begin{aligned} u_R &= \text{sign}(u_{RP})\sqrt{\eta\left[(1 - w_R)\frac{u}{\sin\varepsilon}\left[\left(1 + \frac{1 - K_m}{\zeta}\right)\sin\varepsilon - \frac{1 - K_m}{\zeta}\sqrt{\sin^2\varepsilon + |C_T|}\right]\right]^2 + \text{sign}(u_{RP})(1 - \eta)u_{R0}^2} \\ u_R &= \zeta\,\text{sign}(u_{RP})\sqrt{\left[\eta\left[\left(1 + \frac{1 - K_m}{\zeta}\right)\sin\varepsilon - \frac{1 - K_m}{\zeta}\left(\sqrt{\sin^2\varepsilon + |C_T|}\right)\right]^2 + \text{sign}(u_{RP})(1 - \eta)\sin^2\varepsilon\right] \cdot [(0.7\pi n D_P)^2 + [(1 - w_T)u]^2]} \end{aligned} \tag{9.22}$$

While the second equation of (9.18) can be written as:

$$u_R = \sqrt{\text{sign}(u_{RP})\eta\left[(1-w_R)\frac{u}{\sin\varepsilon}\left[\left(1+\frac{1-K_m}{\zeta}\right)\sin\varepsilon - \frac{1-K_m}{\zeta}\sqrt{\sin^2\varepsilon + |C_T|}\right]\right]^2 + (1-\eta)u_{R0}^2}$$

$$u_R = \zeta\sqrt{\left[\text{sign}(u_{RP})\eta\left[\left(1+\frac{1-K_m}{\zeta}\right)\sin\varepsilon - \frac{1-K_m}{\zeta}\left(\sqrt{\sin^2\varepsilon + |C_T|}\right)\right]^2 + (1-\eta)\sin^2\varepsilon\right] \cdot [(0.7\pi n D_P)^2 + [(1-w_T)u]^2]} \quad (9.23)$$

The conclusion is that for large and small propeller rates (9.22) should be used, while for propeller rates in between (9.23) is applicable.

9.2.2 Limits

In bollard pull conditions, with $u = 0$ and $\sin\varepsilon = 0$, the sign of u_{RP} is negative and equation (9.22) becomes:

$$u_R = 0.7\pi n D_P(1-K_m)\sqrt{\eta|C_T|} \quad (9.24)$$

which does not depend on any wake factor. If the propeller rate is zero, $\sin\varepsilon = 1$ and $\lim_{\varepsilon\to\frac{\pi}{2}} C_T = 0$, the sign of u_{RP} is positive and both equations (9.22) ($\eta \geq 0.5$) or (8.23) ($\eta < 0.5$) become:

$$u_R = (1-w_R)u \quad (9.25)$$

which could be expected. The continuity with the first quadrant is guaranteed.

9.3 Third quadrant

9.3.1 Formulation

In the third quadrant the following expression should be used to evaluate the inflow velocity from the propeller to the rudder:

$$u_{RP} = u_{R0} - (1-K_m)\left(\sqrt{u_p^2\left(1+\left|\frac{8K_T}{\pi J^2}\right|\right)} + u_P\right) \quad (9.26)$$

This can be rewritten as

$$u_{RP} = u\left[(1-w_R) + (1-K_m)(1-w_T)\left(\sqrt{1+\left|\frac{8K_T}{\pi J^2}\right|} - 1\right)\right] \quad (9.27)$$

The weighted average of the inflow velocity in the third quadrant is:

$$u_R = -\sqrt{\eta u_{RP}^2 + (1-\eta)u_{R0}^2} \quad (9.28)$$

Substitution of (9.27) and (9.3) in (9.28) leads to:

$$
\begin{aligned}
u_R &= -\sqrt{\eta\left[u\left[(1-w_R)+(1-K_m)(1-w_T)\left(\sqrt{1+\left|\frac{8K_T}{\pi J^2}\right|}-1\right)\right]\right]^2+(1-\eta)u_{R0}^2} \\
u_R &= u(1-w_R)\sqrt{\eta\left[1-\frac{1-K_m}{\sin\varepsilon}\frac{1-w_T}{1-w_R}\left(\sqrt{\sin^2\varepsilon+|C_T|}+\sin\varepsilon\right)\right]^2+(1-\eta)} \\
u_R &= -(1-w_R)\frac{u}{\sin\varepsilon}\sqrt{\eta\left[-\sin\varepsilon+(1-K_m)\frac{1-w_T}{1-w_R}\left(\sqrt{\sin^2\varepsilon+|C_T|}+\sin\varepsilon\right)\right]^2+(1-\eta)\sin^2\varepsilon}
\end{aligned}
\tag{9.29}
$$

Application of (9.5) and (9.7) results in the following expression for the inflow velocity in the third quadrant:

$$
u_R = -\zeta\sqrt{\left[\eta\left[-\sin\varepsilon+\frac{(1-K_m)}{\zeta}\left(\sqrt{\sin^2\varepsilon+|C_T|}+\sin\varepsilon\right)\right]^2+(1-\eta)\sin^2\varepsilon\right][(0.7\pi nD_P)^2+[(1-w_T)u]^2]}
\tag{9.30}
$$

9.3.2 Limits

In bollard pull conditions, with $u=0$ and $\sin\varepsilon=0$, equation (9.30) transforms into (9.24), so the continuity with the second quadrant is guaranteed. If the propeller rate is zero, with $\sin\varepsilon=-1$ and $\lim_{\varepsilon\to-\frac{\pi}{2}} C_T=0$, (9.30) leads to

$$
\begin{aligned}
u_R &= -\zeta\sqrt{[\eta+(1-\eta)][[(1-w_T)u]^2]} \\
u_R &= -\zeta|(1-w_T)u| \\
u_R &= (1-w_R)u
\end{aligned}
\tag{9.31}
$$

which corresponds to the expected inflow speed.

9.4 Fourth quadrant

9.4.1 Formulation

By smoothly connecting the two valid branches of momentum theory in the vortex ring state region, the inflow speed to the rudder due to propeller action in the fourth quadrant can be written as:

$$
u_{RP}=u_{R0}+K_m\left(\sqrt{u_P^2\left(1+\left|\frac{8K_T}{\pi J^2}\right|\right)}+u_P\right)
\tag{9.32}
$$

or

$$
u_{RP}=u_{R0}-(1-w_T)uK_m\left(\sqrt{1+\left|\frac{8K_T}{\pi J^2}\right|}-1\right)
\tag{9.33}
$$

Depending on the distribution between the ship speed and the propeller rate, the above inflow speed can be either positive or negative. Similar to the second quadrant two possible solutions exist for the global inflow speed:

$$\begin{aligned} u_R &= \text{sign}(u_{RP})\sqrt{\eta u_{RP}^2 - \text{sign}(u_{RP})(1-\eta)u_{R0}^2}; \eta u_{RP}^2 \geq (1-\eta)u_{R0}^2 \\ u_R &= -\sqrt{|\text{sign}(u_{RP})\eta u_{RP}^2 - (1-\eta)u_{R0}^2|}; \eta u_{RP}^2 < (1-\eta)u_{R0}^2 \end{aligned} \tag{9.34}$$

To assess the sign of (9.33) the expression will be rewritten using (9.3) and (9.5):

$$\begin{aligned} u_{RP} &= u\left[1 - w_R - (1-w_T)K_m\left(\sqrt{1 + \left|\frac{C_T}{\sin^2\varepsilon}\right|} - 1\right)\right] \\ u_{RP} &= u\left[1 - w_R + (1-w_T)\frac{K_m}{\sin\varepsilon}\left(\sqrt{\sin^2\varepsilon + |C_T|} + \sin\varepsilon\right)\right] \\ u_{RP} &= (1-w_R)\frac{u}{\sin\varepsilon}\left[\left(1 + \frac{K_m}{\zeta}\right)\sin\varepsilon + \frac{K_m}{\zeta}\left(\sqrt{\sin^2\varepsilon + |C_T|}\right)\right] \end{aligned} \tag{9.35}$$

Or, considering equation (9.7):

$$u_{RP} = \underbrace{\left[(\zeta + K_m)\sin\varepsilon + K_m\sqrt{\sin^2\varepsilon + |C_T|}\right]}_{\leq 0}\underbrace{\sqrt{[(0.7\pi n D_P)^2 + [(1-w_T)u]^2]}}_{\geq 0} \qquad \geq 0 \tag{9.36}$$

The inflow speed u_{RP} is consequently positive when

$$\begin{aligned} u_{RP} &\geq 0 \\ &\Leftrightarrow |(\zeta + K_m)\sin\varepsilon| \leq K_m\sqrt{\sin^2\varepsilon + |C_T|} \\ &\Leftrightarrow |\sin\varepsilon| \leq K_m\sqrt{\frac{|C_T|}{\zeta[\zeta + 2K_m]}} \end{aligned} \tag{9.37}$$

The limiting condition between the two equations in (9.14) can also be rewritten as follows:

$$\begin{aligned} \eta u_{RP}^2 &\geq (1-\eta)u_{R0}^2 \\ &\Leftrightarrow \left[\frac{u}{\sin\varepsilon}\left[\left(1 + \frac{K_m}{\zeta}\right)\sin\varepsilon + \frac{K_m}{\zeta}\sqrt{\sin^2\varepsilon + |C_T|}\right]\right]^2 \geq \frac{1-\eta}{\eta}u^2 \\ &\Leftrightarrow \left|(\zeta + K_m)\sin\varepsilon + K_m\sqrt{\sin^2\varepsilon + |C_T|}\right| \geq \zeta\sqrt{\frac{1-\eta}{\eta}}|\sin\varepsilon| \end{aligned} \tag{9.38}$$

Similar to the second quadrant two sign changes occur for $\eta \geq 0.5$. These sign changes occur when:

$$\begin{aligned} \left|(\zeta + K_m)\sin\varepsilon + K_m\sqrt{\sin^2\varepsilon + |C_T|}\right| &= \zeta\sqrt{\frac{1-\eta}{\eta}}|\sin\varepsilon| \\ &\Leftrightarrow \left[\left(1 + \frac{K_m}{\zeta}\right)\sin\varepsilon + \frac{K_m}{\zeta}\sqrt{\sin^2\varepsilon + |C_T|}\right]^2 = \left[\sqrt{\frac{1-\eta}{\eta}}\sin\varepsilon\right]^2 \\ &\Leftrightarrow A \cdot B = 0 \end{aligned} \tag{9.39}$$

The transitions A and B are given by

$$A = \left(1 + \frac{K_m}{\zeta}\right)\sin\varepsilon + \frac{K_m}{\zeta}\sqrt{\sin^2\varepsilon + |C_T|} + \sqrt{\frac{1-\eta}{\eta}}\sin\varepsilon \tag{9.40}$$

$$B = \left(1 + \frac{K_m}{\zeta}\right)\sin\varepsilon + \frac{K_m}{\zeta}\sqrt{\sin^2\varepsilon + |C_T|} - \sqrt{\frac{1-\eta}{\eta}}\sin\varepsilon \tag{9.41}$$

These equations are equal to zero for:

$$A = 0 \Leftrightarrow \sin\varepsilon = -\frac{K_m}{\zeta}\sqrt{\frac{|C_T|}{\left[1+2\frac{K_m}{\zeta}+\sqrt{\frac{1-\eta}{\eta}}\right]\left[1+\sqrt{\frac{1-\eta}{\eta}}\right]}} \tag{9.42}$$

$$B = 0 \Leftrightarrow \sin\varepsilon = -\frac{K_m}{\zeta}\sqrt{\frac{|C_T|}{\left[1+2\frac{K_m}{\zeta}-\sqrt{\frac{1-\eta}{\eta}}\right]\left[1-\sqrt{\frac{1-\eta}{\eta}}\right]}} \tag{9.43}$$

These equations are implicit, because C_T depends on ε. For large and small propeller rates the first equation of (9.34) is applicable, which can be written as:

$$\begin{aligned} u_R &= \text{sign}(u_{RP})\sqrt{\left(\frac{(1-w_R)u}{\sin\varepsilon}\right)^2\eta\left[\left(1+\frac{K_m}{\zeta}\right)\sin\varepsilon+\frac{K_m}{\zeta}\sqrt{\sin^2\varepsilon+|C_T|}\right]^2-\text{sign}(u_{RP})(1-\eta)\left((1-w_R)u\right)^2} \\ u_R &= \text{sign}(u_{RP})\frac{u}{\sin\varepsilon}\sqrt{(1-w_R)^2\eta\left[\left(1+\frac{K_m}{\zeta}\right)\sin\varepsilon+\frac{K_m}{\zeta}\sqrt{\sin^2\varepsilon+|C_T|}\right]^2-\text{sign}(u_{RP})(1-\eta)\left((1-w_R)\sin\varepsilon\right)^2} \\ u_R &= \text{sign}(u_{RP})(1-w_R)\frac{u}{\sin\varepsilon}\sqrt{\eta\left[\left(1+\frac{K_m}{\zeta}\right)\sin\varepsilon+\frac{K_m}{\zeta}\sqrt{\sin^2\varepsilon+|C_T|}\right]^2-\text{sign}(u_{RP})(1-\eta)\sin^2\varepsilon} \end{aligned} \tag{9.44}$$

$$u_R = \zeta\,\text{sign}(u_{RP})\sqrt{\left[\eta\left[\left(1+\frac{K_m}{\zeta}\right)\sin\varepsilon+\frac{K_m}{\zeta}\left(\sqrt{\sin^2\varepsilon+|C_T|}\right)\right]^2-\text{sign}(u_{RP})(1-\eta)\sin^2\varepsilon\right]\cdot\left[(0.7\pi nD_P)^2+[(1-w_T)u]^2\right]} \tag{9.45}$$

While for intermediate propeller rates the second equation of (9.34) should be used

$$\begin{aligned} u_R &= -\sqrt{\left|\left(\frac{(1-w_R)u}{\sin\varepsilon}\right)^2\text{sign}(u_{RP})\eta\left[\left(1+\frac{K_m}{\zeta}\right)\sin\varepsilon+\frac{K_m}{\zeta}\sqrt{\sin^2\varepsilon+|C_T|}\right]^2-(1-\eta)\left((1-w_R)u\right)^2\right|} \\ u_R &= -(1-w_R)\frac{u}{\sin\varepsilon}\sqrt{\left|\text{sign}(u_{RP})\eta\left[\left(1+\frac{K_m}{\zeta}\right)\sin\varepsilon+\frac{K_m}{\zeta}\sqrt{\sin^2\varepsilon+|C_T|}\right]^2-(1-\eta)\sin^2\varepsilon\right|} \\ u_R &= -(1-w_R)\frac{\sqrt{(0.7\pi nD_P)^2+u_P^2}}{1-w_T}\sqrt{\left|\text{sign}(u_{RP})\eta\left[\left(1+\frac{K_m}{\zeta}\right)\sin\varepsilon+\frac{K_m}{\zeta}\sqrt{\sin^2\varepsilon+|C_T|}\right]^2-(1-\eta)\sin^2\varepsilon\right|} \end{aligned} \tag{9.46}$$

$$u_R = -\zeta\sqrt{\left|\text{sign}(u_{RP})\eta\left[\left(1+\frac{K_m}{\zeta}\right)\sin\varepsilon+\frac{K_m}{\zeta}\left(\sqrt{\sin^2\varepsilon+|C_T|}\right)\right]^2-(1-\eta)\sin^2\varepsilon\right|\cdot\left[(0.7\pi nD_P)^2+[(1-w_T)u]^2\right]} \tag{9.47}$$

9.4.2 Limits

According to (9.37) u_{RP} is strictly positive in bollard pull conditions and considering $u = 0$, $\sin\varepsilon = 0$, (9.45) can be transformed to

$$u_R = 0.7\pi nD_P K_m\sqrt{\eta C_T} \tag{9.48}$$

which corresponds to the limit obtained in the first quadrant. If n equals zero the sign of u_{RP} is always negative. Depending on the value of η (9.45) or (9.47) should be evaluated with $n = 0$ and $\sin\varepsilon = -1$, which leads in both cases to

$$u_R = (1 - w_R)u \tag{9.49}$$

and proves the continuity with the third quadrant.

10 Appendix 2: symmetry considerations

For simulation purposes it is convenient to build a symmetric model, so that symmetric manoeuvres will lead to symmetric results for ships equipped with twin rudders and twin propellers. To set the ideas, the longitudinal inflow speed to a portside rudder in the first quadrant is, for its lateral force:

$$u_{R,PS} = \zeta_{PS}(\varepsilon^*)\sqrt{\left[\eta_{PS}\left[\left(1 - \frac{K_{m,PS}(\delta_{PS})}{\zeta_{PS}(\varepsilon^*)}\right)\sin\varepsilon + \frac{K_{m,PS}(\delta_{PS})}{\zeta_{PS}(\varepsilon^*)}\left(\sqrt{\sin^2\varepsilon + C_T}\right)\right]^2 + (1 - \eta_{PS})\sin^2\varepsilon\right] \cdot \left[(0.7\pi n D_P)^2 + \left[\left(1 - w_T(\varepsilon^*)\right)u\right]^2\right]} \tag{10.1}$$

The same longitudinal inflow speed should be obtained to the starboard side rudder when its angle is put at $\delta_{SS} = -\delta_{PS}$. This is the case when:

- $\eta_{PS} = \eta_{SS}$;
- $\zeta_{PS}(\varepsilon^*) = \zeta_{SS}(\varepsilon^*)$;
- $K_{m,PS}(\delta_{PS}) = K_{m,SS}(-\delta_{PS})$.

The lateral inflow speed to the portside rudder is:

$$v_{R,PS} = k_{Hv,PS}(\beta)v - k_{Hr,PS}(\gamma)r\frac{L_{PP}}{2} \tag{10.2}$$

The same magnitude of the lateral inflow speed should be obtained to the starboard side rudder when the drift and yaw angle are opposite, thus:

- $k_{Hv,PS}(\beta) = k_{Hv,SS}(-\beta)$;
- $k_{Hr,PS}(\gamma) = k_{Hr,SS}(-\gamma)$.

The net rudder angles should be equal as well, which means:

- $\delta_{0,PS} = -\delta_{0,SS}$.

However, this is problematic if both the portside and starboard side neutral rudder angle have the same sign. In such case, it is preferable to assume that:

- $\delta_{0,PS} = 0 = \delta_{0,SS}$.

With the above the inflow conditions are symmetric, but the rudder forces will only be symmetric when the open water characteristics are symmetric as well:

- $C_{L,PS}(\alpha) = C_{L,SS}(-\alpha)$;
- $C_{D,PS}(\alpha) = C_{D,SS}(-\alpha)$.